PRETREATMENT OF RED GYPSUM FOR VALUE-ADDED APPLICATION

SUN JIAN MENG

A project report submitted in partial fulfilment of the requirements for the award of Bachelor of Engineering (Honours) Chemical Engineering

Lee Kong Chian Faculty of Engineering and Science
Universiti Tunku Abdul Rahman

May 2022

DECLARATION

I hereby declare that this project report is based on my original work except for citations and quotations which have been duly acknowledged. I also declare that it has not been previously and concurrently submitted for any other degree or award at UTAR or other institutions.

Signature   :

Name   : SUN JIAN MENG

ID No.   : 18UEB03192

Date   : 16th May 2022

APPROVAL FOR SUBMISSION

I certify that this project report entitled **"PRETREATMENT OF RED GYPSUM FOR VALUE-ADDED APPLICATION"** was prepared by **SUN JIAN MENG** has met the required standard for submission in partial fulfilment of the requirements for the award of Bachelor of Engineering (Honours) Chemical Engineering at Universiti Tunku Abdul Rahman.

Approved by,

Signature   :   *steven*

Supervisor   :   Dr. Steven Lim

Date   :   16th May 2022

Signature   :

Co-Supervisor :

Date   :

The copyright of this report belongs to the author under the terms of the copyright Act 1987 as qualified by Intellectual Property Policy of Universiti Tunku Abdul Rahman. Due acknowledgement shall always be made of the use of any material contained in, or derived from, this report.

ACKNOWLEDGEMENTS

I would like to thank everyone who had contributed to the successful completion of this project. I would like to express my gratitude to my research supervisor, Dr. Steven Lim for his invaluable advice, guidance, and enormous patience throughout the research development.

In addition, I would also like to express my gratitude to my loving parents and friends who had helped and given me encouragement in completing this report. Without them, I would not have resolved the problems I faced during my research work and report writing.

ABSTRACT

Red gypsum is a mineral-rich in iron and it is the by-product of the sulfuric acid process of the Ilmenite-based industrial titanium dioxide process. The characterisation of red gypsum is reviewed in this study. It was found that the presence of iron sulphate in red gypsum is one of the impurities that restricted its reutilization. The implementation of the pretreatment method for red gypsum separation is to reduce disposal to the landfills. At the same time, the products which should be natural gypsum can proceed into a value-added application such as cement production. Three pretreatment methods that do not require complicated equipment setup and have simplified procedures are studied: mineral carbonation, acid leaching and hydrothermal treatment. These pretreatment methods are reviewed based on their objective, material and equipment used, parameter studies, mechanisms, and feasibility. The efficiency of mineral carbonation, acid leaching and hydrothermal methods were 26.31% (70 bar of CO_2 pressure, less than 45 μm of particle size and 200 ℃ of temperature), 93.14% (0.5 M of concentration of H_2SO_4, 60 minutes of reaction time, 70 ℃ of temperature and 1:12.5 g/mL of solid-liquid ratio) and 99% (1.5 M HCl as mineraliser, 10 mL/g of liquid-solid ratio, 6 hours of reaction time and 140 ℃ of temperature), respectively. Besides, the material and energy costs of three pretreatment methods were also performed in this study. The total cost required for mineral carbonation, acid leaching and hydrothermal methods were RM 13040.41, RM 5460.32 and RM 6461.85, respectively. The justification of the best pretreatment method for red gypsum separation was based on environmental, cost and efficiency perspectives. This study showed that the mineral carbonation method is an environmentally friendly method to store carbon dioxide in solid carbonates. However, the efficiency of this method was very low, so the products cannot be used for other applications as the impurity content was still high. Although the cost required for the acid leaching method was lower than hydrothermal treatment, the purity of products for hydrothermal treatment was higher. Therefore, the overall products' benefit would be higher than the acid leaching method. As a result, the best pretreatment method for red gypsum separation is the hydrothermal treatment method.

TABLE OF CONTENTS

LIST OF TABLES

LIST OF FIGURES

LIST OF SYMBOLS / ABBREVIATIONS

$\left(C_{pa}\right)_C$	atomic heat capacity of calcium, J/(g·atom·°C)
$\left(C_{pa}\right)_O$	atomic heat capacity of oxygen, J/(g·atom·°C)
ΔP	differential pressure, psi
d	diffraction peak, Å
F	flowrate, gpm
$\left(C_p\right)_{CO_2}$	heat capacity of CO_2 liquid, J/(mol·°C)
X	iron or calcium in red gypsum
M_2	molarity of dilute acid, M
M_1	molarity of purchase acid, M
MW_X	molecular weight of iron or calcium, g/mol
P	power. Hp
P_{XCO_3}	purity of product, %
V_2	volume of dilute acid, ml
V_1	volume of purchase acid, ml
ΔW	weight loss of sample, kg

CH_3COOH	acetic acid
Al	aluminium
$Al(OH)_3$	aluminium hydroxide
Al_2O_3	aluminium oxide
AASHTO	American Association of State Highway and Transportation Officials
ASTM	American Society for Testing Materials
$(NH_4)_2CO_3$	ammonium carbonate
NH_4OH	ammonium hydroxide
AH	anhydrous
BaO	barium oxide
HCO_3^-	bicarbonate ion
$HSO4^-$	bisulphate ion
Ca	calcium
Ca^{2+}	calcium ion

$CaCO_3$	calcium carbonate
$Ca(OH)_2$	calcium hydroxide
CaO	calcium oxide
$CaSO_4$	calcium sulphate
$CaSO_4 \cdot 2H_2O$	calcium sulphate dihydrate
$CaSO_4 \cdot 0.5H_2O$	calcium sulphate hemihydrate
CBR	Californian bearing ratio, %
CCS	carbon capture and storage
CO_2	carbon dioxide
CO_3^{2-}	carbonate ion
H_2CO_3	carbonic acid
CEC	cation exchange capacity, meq/100g
CNY	Chinese yuan renminbi
Cl	chlorine
CrO_4^{2-}	chromate ion
Cr(VI)	chromium hexavalent ion
CAGR	compound annual growth rate
$Cr_2O_7^{2-}$	dichromate ion
DH	dihydrate
$Fe(OH)_3$	ferric hydroxide
Fe^{3+}	ferric ion
Fe_2O_3	ferric oxide
$Fe_2(SO_4)_3$	ferric sulphate
$FeCO_3$	ferrous carbonate
$Fe(OH)_2$	ferrous hydroxide
Fe^{2+}	ferrous ion
$FeSO_4$	ferrous sulphate
FGD	flue gas desulphurisation
HCOOH	formic acid
FTIR	Fourier Transform Infrared Spectroscopy
GHG	global greenhouse gases
HH	hemihydrate
HPHT	high pressure high temperature
HCl	hydrochloric acid

H^+	hydrogen ion
HTT	hydrothermal treatment
$FeTiO_3$	ilmenite ore
Pb	lead
LL	liquid limit, %
L/S	liquid-solid
Mg	magnesium
Mg^{2+}	magnesium ion
$MgCO_3$	magnesium carbonate
$Mg(OH)_2$	magnesium hydroxide
MgO	magnesium oxide
Mn	manganese
MnO	manganese(II) oxide
NIST	National Institute of Standards and Technology
NORM	naturally occurring radioactive materials
HNO_3	nitric acid
O_2	oxygen gas
P_2O_5	phosphorus pentoxide
PL	plastic limit, %
Po	polonium
K	potassium
KOH	potassium hydroxide
K_2O	potassium oxide
Ra	radium
RG	red gypsum
SEPA	Scottish Environment Protection Agency
SEM-EDX	scanning electron microscope coupled with energy dispersive X-ray
SL	shrinkage limit, %
Si	silicon
SiO_2	silicon dioxide
NaOH	sodium hydroxide
Na_2O	sodium oxide
S/L	solid-liquid

SO_4^{2-}	sulphate ion
S	sulphur
SO_3	sulphur trioxide
H_2SO_4	sulphuric acid
Th	thorium
TiO_2	titanium dioxide
U	uranium
H_2O	water
XRD	X-ray diffractometer
XRF	X-ray fluorescence
ZnO	zinc oxide
ZrO_2	zirconium dioxide

LIST OF APPENDICES

CHAPTER 1

INTRODUCTION

1.1   General Introduction

Red gypsum (RG) is a solid residue waste primarily constituted of calcium sulphate dihydrate ($CaSO_4 \cdot 2H_2O$), iron hydroxide ($Fe(OH)_2$) and a small amount of aluminium hydroxide ($Al(OH)_3$) formed during the sulphuric acid process of titanium dioxide, TiO_2 manufacturing (Chen, et al., 2021). In other words, it is a form of iron-rich gypsum residue produced by the ilmenite-based industrial titanium dioxide production (Peng, et al., 2021). The sulphate process is used in manufacturing titanium dioxide, including reacting sulphuric acid with ilmenite ore, followed by purifying and calcination techniques to produce titanium dioxide pigment. The sulphuric acid wastes produced from the sulphate process required a costly neutralisation treatment before the wastes could be disposed of (Azdarpour, et al., 2014). In the neutralisation treatment, lime or limestone is used to neutralise the excess sulphuric acid solution (H_2SO_4) and iron sulphate ($FeSO_4$), resulting in the by-product red gypsum, which is mainly composed of gypsum and iron hydroxides. Figure 1.1 shows the production of RG in the sulphate process of TiO_2 production (Gázquez, et al., 2009). The illustration of the reaction is shown in Equations 1.1 and 1.2.

$$Ca(OH)_2 + H_2SO_4 \rightarrow CaSO_4 \cdot 2H_2O \qquad (1.1)$$

$$FeSO_4 + Ca(OH)_2 \rightarrow Fe(OH)_2 + CaSO_4 \qquad (1.2)$$
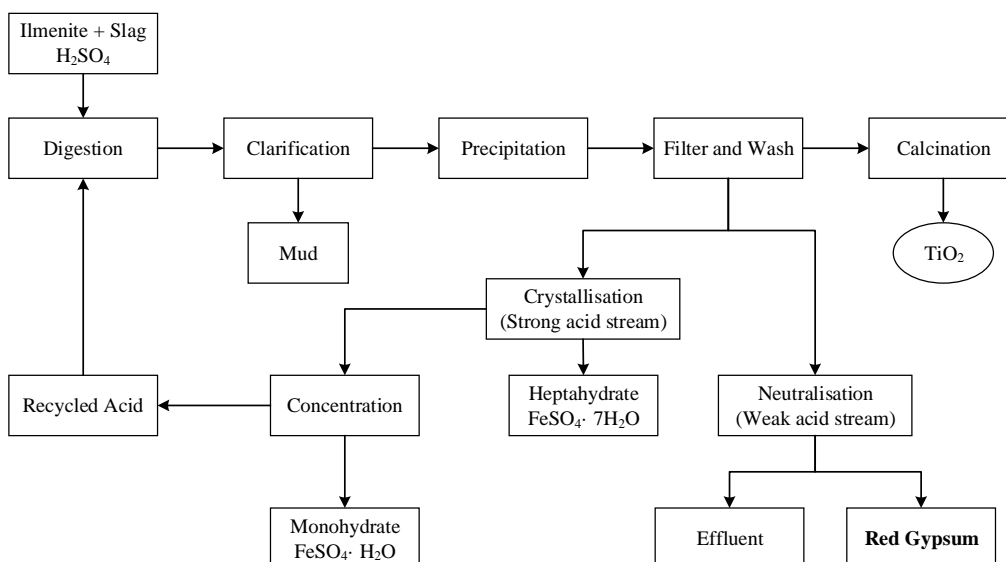
Figure 1.1: Production of RG in Sulphate Process of TiO$_2$ Production
(Gázquez, et al., 2009).

Approximately 5 – 7 tonnes of RG are produced for every tonne of titanium dioxide. Annually, almost 15 million tonnes of RG are produced in China (Chen, et al., 2021). In Malaysia, the capacity of the Huntsman Tioxide plant, one of the largest producers of TiO$_2$ pigments, is approximately 56 000 metric tonnes annually and at least 340 000 tonnes of RG have accumulated annually (Azdarpour, et al., 2014; Kamarudin and Zakaria, 2007). Furthermore, RG generated in the Huelva (southwestern Spain) produces over 70 000 tonnes each year and disposes it in a supervised industrial waste landfill around 70 kilometres from the factory (Gazquez et al., 2013). Therefore, the majority of RG is commonly stacked or landfilled around the TiO$_2$ pigments plant. Biodegradable waste will mix with RG in landfills, resulting in hydrogen sulphate gas emissions. Additionally, hydrogen sulphide is poisonous, colourless, and combustible, with a distinct rotten egg odour that can cause breathing difficulty, skin discolouration and eye irritation (Hamid, et al., 2021). Therefore, RG as an industrial waste takes up massive amounts of land, pollutes the environment, and puts the public's health in jeopardy (Zhang, et al., 2016).

In order to reduce environmental and human harm, some researchers investigated the comprehensive utilisation of RG from the following

perspectives: commercial cement retarder production (Zhang, et al., 2019), preparation of materials for wall construction (Wu, et al., 2019), usage as a soil amendment (Fauziah, Zauyah and Jamal, 1996), usage as raw materials for mineral carbonation (Azdarpour, et al., 2014) and production of glazes in the ceramic industry (Kamarudin and Zakaria, 2007).

In recent years, red gypsum treatment technology has included cement-based composites made of RG instead of natural gypsum, which can accomplish resource utilisation goals. However, the use of RG as a cement retarder to replace natural gypsum is restricted. In general, RG has a lower dose as a cement retarder, making it unable to achieve the massive consumption target. Its manufacturing performance is somewhat inferior to that of natural gypsum. The variations in moisture and impurity contents can alter the cement's setting and hardening (Wu, et al., 2019). Besides, the impurity contents can affect moisture absorption, defrost and the whiteness of cement. Among the impurity contents, $FeSO_4$ can reduce the mechanical strength of the cement and significantly affect the physical properties of cement (Jiang, Sun and Peng, 2019). The high iron impurity level will affect cement production, resulting in low product's whiteness and poor mechanical qualities of gypsum blocks, limiting RG application in construction materials and other industries (Peng, et al., 2021). Thus, it is crucial to extract the iron metal impurities from the red gypsum.

Several methods can be used to treat the RG into natural gypsum, which includes production of solid carbonation by mineral carbonating red gypsum (Azdarpour, et al., 2014), hydrothermal treatment with an acid method (Peng, et al., 2021), acid leaching method (Azdarpour, et al., 2015), reduction method by using carbon as a reducing agent (Clark, 2005) and metal self-enrichment process (Wu, et al., 2019), a combination of reduction method and magnetic method (Ding et al., 2016).

1.2   Importance of the Study

From the year 2021 to the year 2028, the entire titanium dioxide market is expected to increase at a compound annual growth rate (CAGR) of 8.3%. The increase in product demand from end-user industries can be attributed to this rise (InkWorld, 2021). As RG is one of the by-products in titanium dioxide

manufacturing, the quantity of RG will be increased in the next few years. RG is an industrial waste that is harmful to both environment and humans as it has high iron impurity levels. RG is produced in great quantity by TiO_2 pigment plants. If these numerous RG are not reutilised in industrial applications, it will be disposed to landfills. Landfills can significantly affect the air pollution, nature, the environment, and humans. Besides, chemicals or toxic substances from landfills may be saturating the soil in the region (Newton, 2018). Additionally, RG contains chemical material that kills the plantation and pollutes the water. The heavy metals in RG will be absorbed by the plant or flow into groundwater (Fauziah, Zauyah and Jamal, 1996). After extracting the iron metal impurities from RG, it becomes natural gypsum. Natural gypsum has a wide range of industrial applications based on its calcined forms, such as retarder for fertilizer, cement, mineral filler, soil conditioner, oxidizing agent in glass production, et cetera (Artha Mineral Resources, 2021). Therefore, by reducing negative environmental impact and increasing the value of RG, an analytical study of various pretreatment methods of RG for value-added application is essential.

1.3 Problem Statement

Environmental concerns have directed substantial interest in reducing industrial wastes. RG is one of the inevitable industrial wastes from the production of TiO_2 pigment plants. When the RG waste is in excess, the red gypsum will be disposed of in the landfill, causing many environmental problems, including the emission of hydrogen sulphate gas, killing the plantation and polluting the groundwater. Therefore, RG must be dumped in a separate container or cell that does not accept biodegradable waste (Scottish Environment Protection Agency (SEPA), 2009). Besides, RG without any treatment has the characteristics of high-water content, high viscosity and high impurity content. The excessive RG occupies a lot of lands, pollutes the environment, and causes a substantial economic burden to titanium dioxide enterprises. Currently, many pretreatment methods are used to treat RG into natural gypsum and utilise it in various industrial applications. However, some of these existing techniques or technologies have a number of drawbacks, including high costs of the process, complex procedures, lack of

environmental protection, low iron oxide extraction efficiency and the potential for secondary pollution. For example, sodium dithionite is used to reduce Fe^{3+} ions into Fe^{2+} ions, which is soluble in water to obtain natural gypsum. The cost of this process is high, other impurities are introduced, and it is easy to cause pollution to the environment (Jiang, Sun and Peng, 2019). Thus, in order to determine the best pretreatment method for extracting iron metal from RG with the least cost, high efficiency and low environmental negative impact, three methods (mineral carbonation method, acid leaching method and hydrothermal treatment method) were analysed in detail.

1.4   Aim and Objectives

The primary aim of this study is to look into the pretreatment of red gypsum for value-added application with the following objectives to be achieved:

     i.   To analyse the characterisation of red gypsum and the existing technologies for red gypsum separation.

     ii.   To perform material and energy cost analysis on existing technologies.

     iii.   To justify the best pretreatment method for red gypsum separation.

1.5   Scope and Limitations of the Study

First of all, one of the scopes of this study is to review current technologies for separating iron metal from red gypsum. Three selected technologies are mineral carbonation of red gypsum, acid leaching and hydrothermal treatment methods. Besides, the characterisation properties of red gypsums, such as composition, physical property, chemical property, crystalline phases, surface morphologies and microstructure, as well as radiological characterisation, are reviewed in this study. Furthermore, material and energy costs for each technology are performed in this study as well. Finally, the justification of the best pretreatment method for red gypsum is discussed based on three aspects: environmental, efficiency and cost.

However, there are some limitations to this study. Firstly, the technologies reviewed are based on the laboratory scale. Secondly, the cost analysis is not being considered for the cost of equipment. Thirdly, this study

is not verified by through experimental works but just reviewed based on other researchers' experiments.

1.6 Outline of the Report

Chapter 1 briefly introduces TiO_2 production that produces red gypsum as a by-product, its production capacity, its negative impact on numerous industrial waste (red gypsum) and the study's problem statement, aim and objectives. After that, the characterisation properties of red gypsum will be reviewed in Chapter 2. In the same chapter, the details, including material and equipment used, parameters study, mechanism and feasibility study of three treatment methods (mineral carbonation method, acid leaching method and hydrothermal treatment method) will be reviewed. The methodology of reviewing the literature, obtaining the data, performing and presenting the results are included in Chapter 3. Chapter 4 included the cost analysis and justification of the best pretreatment method while Chapter 5 provides a brief conclusion of this study and recommendations for further studies.

CHAPTER 2

LITERATURE REVIEW

2.1   Introduction

Many studies have been conducted to date on the pretreatment of red gypsum in order to remove iron impurities and produce natural gypsum (Azdarpour et al., 2014; Rahmani, Tyrer and Junin, 2014; Jiang, Sun and Peng, 2019; Azdarpour et al., 2015; Peng et al., 2021). The analysis of the achievement on the justification of the best method for pretreatment of red gypsum can be guided by examining related papers from earlier years.

2.2   Characterisation Properties of Red Gypsum

2.2.1   Composition of Red Gypsum

X-ray fluorescence (XRF) is equipment that can be used to determine the major components in RG. Table 2.1 shows the XRF analysis results of the RG. It can be seen that the main chemical components of RG are SO_3 (32.39%), CaO (26.36%), Fe_2O_3 (16.04%), SiO_2 (1.50%), containing a small amount of Al_2O_3, MgO, TiO_2, MnO, P_2O_5 and Cl, and trace number of Na_2O, BaO, K_2O. The ignition loss was found to be as high as 20.39% (Jiang, Sun and Peng, 2019; Chen, et al., 2021).

Table 2.1: Chemical Composition of the RG (Jiang, Sun and Peng, 2019; Chen et al., 2021).

Compound	Concentration (wt%)
SO_3	32.39
CaO	26.36
Fe_2O_3	16.04
SiO_2	1.50
Al_2O_3	0.98
MgO	0.82
TiO_2	0.76
MnO	0.32

Table 2.1 (Continued)

Compound	Concentration (wt%)
P_2O_5	0.14
Cl	0.13
Na_2O	0.07
BaO	0.04
K_2O	0.02
ZnO	0.01
ZrO_2	0.01
LOSS	20.39
TOTAL	99.99

2.2.2 Physical and Chemical Properties of Red Gypsum

Ilmenite (titanium and iron-rich mineral) is used as a raw material in the production of titanium dioxide pigments with the "sulphate method" is generating the by-product, red gypsum (RG), a reddish-brown semi-solid mud as mentioned in **Chapter 1**. As sulphuric acid is used in the production, resulting RG has a high concentration of CaO and SO_3, with $CaSO_4 \cdot 2H_2O$ as the predominant crystalline phase (Gazquez, et al., 2013). Besides, iron hydroxide is also one of the major constituents of RG. It is the key contributing element to the reddish-brown appearance of RG. In addition, high iron concentration in RG results in essential mineral properties for water retention ability, carbonation reaction, high free swell index and low permeability (Mahazam and Mohd Azmi, 2016). Table 2.2 shows RG's physical and chemical properties and its testing methods, while Table 2.3 shows the properties of RG without providing testing methods.

Table 2.2: Physical and Chemical Properties of RG and Its Testing Method
(Mahazam and Mohd Azmi, 2016).

Physical Properties	Results	Testing Method
Specific Gravity	3.16	Small Pycnometer Method (British Standard, 1990 p.2)

Table 2.2 (Continued)

Physical Properties	Results	Testing Method
Particle Size Distribution	Clay	Dry Sieving Method and Sedimentation by the Hydrometer Method (British Standard, 1990 p.2)
Liquid limit, LL (%)	91.97	Cone Penetrometer Method or Definitive Method (British Standard, 1990 p.2)
Plastic Limit, PL (%)	58.28	Method for Plastic Limit (British Standard, 1990 p.2)
Shrinkage Limit, SL (%)	17.50	Wax Method (ASTM Standard, 2008)
Water content (%)	17.25	Oven-drying Method (British Standard, 1990 p.2)
Specific Surface Area (m^2/g)	814.72	Ethylene Glycol Monoethyl Ether (EGME) Retention Method
Swell Index, C_s (%)	180	Not Available
Chemical Properties	**Results**	**Testing Method**
Cation Exchange Capacity (CEC) (meq/100g)	1.243	Ammonium Acetate Method

Table 2.3: Properties of RG without Providing Testing Methods (Tooze, Noble and August, 2003).

Properties	Results
pH	7.4
Free Moisture (%)	10 – 50
Particle Density (mg/m^3)	2.71
Dry Density (mg/m^3)	1.21
Erodibility (Dispersiveness)	Dispersive 4
Californian Bearing Ratio, CBR (%)	23.05
Optimum Moisture Content (%)	41
Coefficient of Volume Change, M_v (m^2/MN)	0.907 – 0.179
Coefficient of Consolidation, C_v (m^2/year)	0.855 – 0.232

Table 2.3 (Continued)

Properties	Results
Coefficient of Secondary Compression, C_α (m^2/year)	0.004 – 0.002
Compression Index, C_C	0.242
Permeability, $k_v \times 10^{-9}$ (m/s)	3.314 – 6.92
Undrained Shear Strength, C_u (kN/m^2)	194 – 355
Strain to Failure (%)	10

According to the findings, RG has a high specific gravity, which could be attributed to the presence of iron in the RG, which would normally cause a high specific gravity in the range of 2.75 to 3.0 or even higher (ASTM Standard, 2002). In the perspective of particle size determinations, RG may need to be pastel carefully without breaking down its crystal. Although oven drying eliminates cohesive force as water evaporates, RG is a form of clay that readily absorbs moisture from the atmosphere or surroundings, resulting in the soil wet and difficult to sieve. RG passes through a 2 mm sieve with a reasonable passage during the crushing process. Its liquid limit (LL) and plastic limit (PL) indicate that RG is a form of clay, according to the American Association of State Highway and Transportation Officials (AASHTO) soil classification chart. The specific surface area of RG per gram is significant, indicating that the RG particle has a high-water retention capacity and is a fine particle. The free swell index of RG is likewise exceptionally high, indicating that it is expansive soil, while the SL indicates that RG will shrink greatly when dried out. The cation exchange capacity (CEC) was only 1.243 meq/100g, indicating that the soil has a lower negative charge, fewer cations that can be stored, and less organic matter (Mahazam and Mohd Azmi, 2016).

2.2.3 Crystalline Phases of Red Gypsum

The crystalline phases of RG can be determined using X-ray Diffractometer (XRD), and the XRD pattern of RG is shown in Figure 2.1. The analysis shows that the main phase of RG is dihydrate (DH) gypsum (CaSO$_4$·2H$_2$O), and its main characteristic diffraction peaks are $d_{020} = 7.6346$Å, $d_{021} = 4.2896$Å, $d_{041} = 3.0674$Å and $d_{-221} = 2.8735$Å. However, the XRD pattern

does not detect the characteristic diffraction peaks containing iron metal, indicating that the iron oxide components in the RG mainly exist in an amorphous state (Jiang, Sun and Peng, 2019). Aside from that, Pérez-Moreno, Gázquez and Bolívar (2015) also concluded that the major crystalline phases discovered in red gypsum were primarily composed of DH gypsum, approximately 90%, which was consistent with earlier findings.
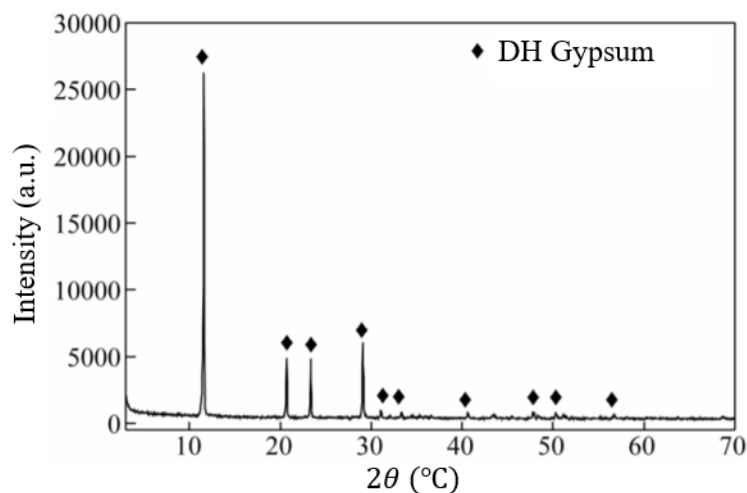
Figure 2.1: XRD Pattern of Red Gypsum (Jiang, Sun and Peng, 2019).

Azdarpour, et al. (2015) concluded that the XRD pattern showed four peaks that were attributed to DH gypsum in red gypsum at 11.68°, 20.79°, 23.44° and 29.16°, which is shown in Figure 2.2. Besides, five additional peaks at 35.41°, 40.64°, 47.84°, 50.34°, and 51.18° were assigned to iron oxide. These data are in good accordance with the reported data in articles by Fauziah, Zauyah and Jamal (1996), Sahoo, et al. (2011), Benhammada, et al. (2020) and Chen, et al. (2014). Figure 2.1 and Figure 2.2 differ because the RG was from different ilmenite-based industrial titanium dioxide production, so that it might compose different crystalline phases of RG.
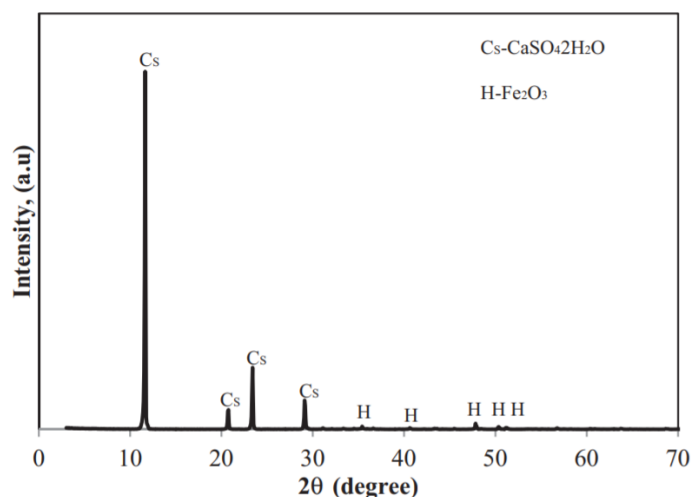
Figure 2.2: XRD Pattern of Red Gypsum (Azdarpour, et al., 2015).

2.2.4 Surface Morphologies and Microstructures of Red Gypsum

Figure 2.3 shows the surface morphologies and microstructures of red gypsum using a Scanning Electron Microscope coupled with Energy Dispersive X-ray (SEM-EDX) equipment. It can be observed that there are three different shapes, including strips, plate-shaped particles, and irregular blocks. Furthermore, the fine particle aggregation, numerous surface flaws, and a significant number of particles debris adsorbed on the rough surface of blocks can be seen clearly (Peng, et al., 2021). According to Jiang, Sun and Peng (2019), RG includes two types of particles, the long or plate-shaped particles of different sizes are DH gypsum crystals, and the irregular fine particles or agglomerates are mainly iron hydroxides.

Furthermore, Gázquez, et al. (2009) also examined tubular and prismatic crystals with extended morphologies, and symmetrical crystal groups with varied orientations in the RG secondary electron image produced by SEM as shown in Figure 2.4. The accompanying EDX spectra showed that RG was mostly made up of Ca and S.

Based on Figure 2.4, the major components of RG are standard gypsum crystals that include iron which can be seen in point 1. However, there are small particles, also called amorphous material, deposited onto $CaSO_4$ crystals that contain high concentrations of iron or a high amount of titanium as shown in point 2. Various metals such as Si, Mn, Al, Mg and others are detected by XRF analysis in point 3 (Gázquez, et al., 2009).
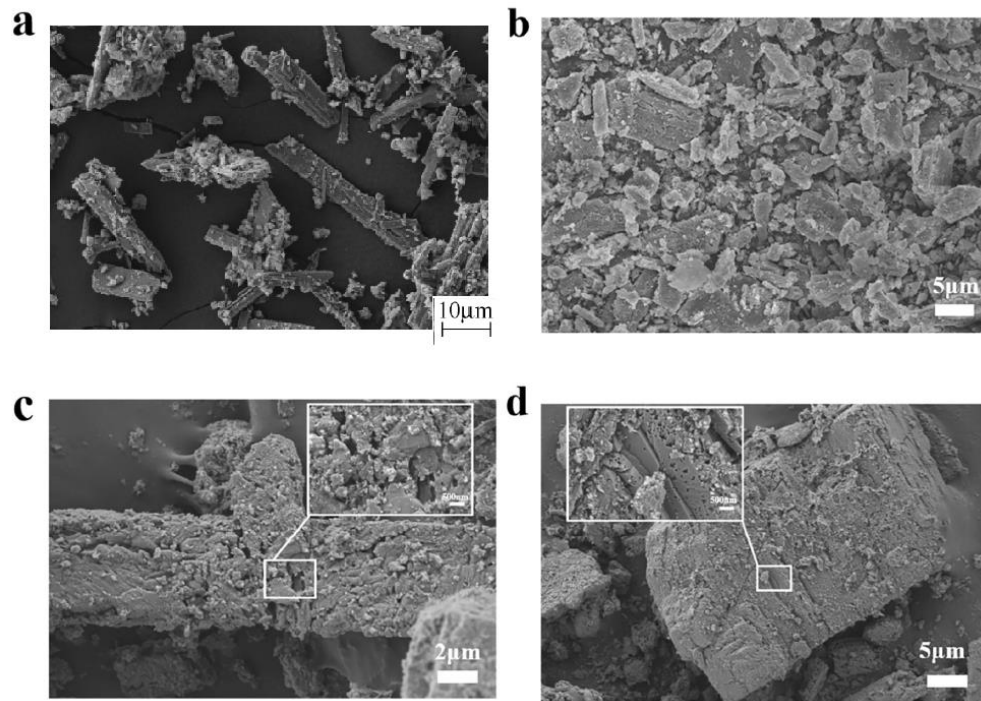
Figure 2.3: SEM Image of Red Gypsum (Peng, et al., 2021; Jiang, Sun and
Peng, 2019).
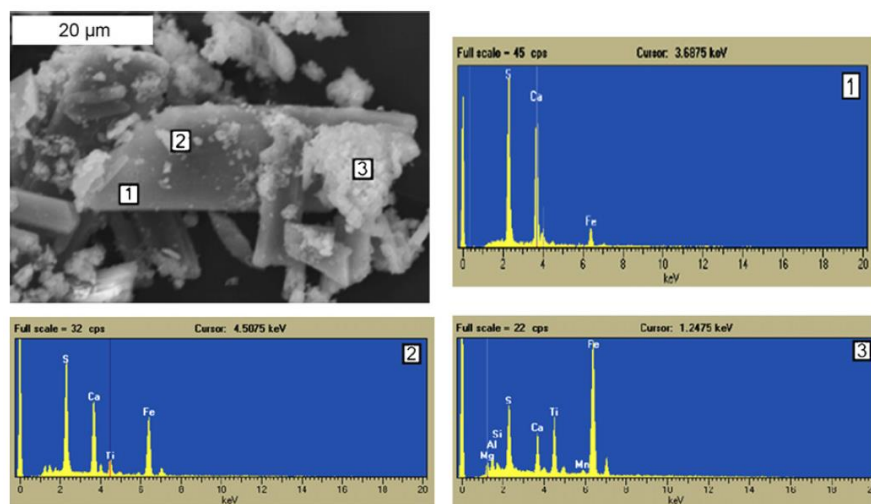
Figure 2.4: Secondary Electron SEM study of RG and its associated X-ray
Spectra (Gázquez, et al., 2009).

2.2.5 Radiological Characterisation

In the research of Mantero, et al. (2013) and Gázquez, et al. (2011), they showed that the manufacturing of titanium dioxide is a Naturally Occurring Radioactive Materials (NORM) industry as the raw material utilised in the industrial process is ilmenite. Ilmenite is a mineral ore enriched in natural radionuclides from the uranium (U-), thorium (Th-) series and ^{40}K. In order to establish the environmental impacts of RG, a radiological study is required. Table 2.4 shows the radionuclides activity concentrations from thorium and uranium series with half-lives more than one month of ilmenite and red gypsum from different literature.

Table 2.4: Activity Concentrations of Radionuclide of Ilmenite and Red Gypsum from Different Sources (Gázquez, et al., 2011; Pérez-Moreno, Gázquez and Bolívar, 2015; Mantero, et al., 2013).

Radionuclide	Concentrations (Bq/kg)			
	Ilmenite		Red Gypsum	
	(Gázquez, et al., 2011)	(Mantero, et al., 2013)	(Mantero, et al., 2013)	(Pérez-Moreno, Gázquez and Bolívar, 2015)
^{238}U	119 ± 3	119 ± 3	15 ± 1	16 ± 1
^{234}U	129 ± 5	129 ± 5	18 ± 1	18 ± 1
^{230}Th	85 ± 5	85 ± 5	41 ± 2	32 ± 2
^{226}Ra	86 ± 5	92 ± 5	13 ± 2	14 ± 2
^{232}Th	315 ± 20	315 ± 20	143 ± 5	138 ± 4
^{228}Ra	301 ± 20	301 ± 20	69 ± 5	-
^{228}Th	305 ± 23	305 ± 23	93 ± 6	-
^{210}Po	-	-	-	27 ± 1
^{210}Pb	-	94 ± 15	24 ± 4	-
^{40}K	20.2 ± 2.2	20 ± 2	24 ± 9	19 ± 6

The first thing that can be noticed from Table 2.4 is that all of the values coupled with the mean deviations are less than 16 percent, indicating that the samples are quite homogeneous in terms of radioactivity. Ilmenite is

likewise a NORM mineral since it is enriched in natural radionuclides from both the uranium (U-) and thorium (Th-) series (in secular equilibrium), with a total concentration of 434 Bq/kg for the ^{238}U and ^{232}Th nuclides (Gázquez, et al., 2011).

As shown in Figure 1.1, the red gypsum is formed from the neutralisation process. Despite accumulating the majority of the radioactive content originally associated with acid waters, RG has moderate activity levels of radioactivity as shown in Table 2.4. The radionuclides in acid waters are diluted in gypsum, which is generated from calcium hydroxide ($Ca(OH)_2$) and magnesium hydroxides ($Mg(OH)_2$) and contains very low activity concentrations in radionuclides from the uranium and thorium series. Therefore, a small portion of the natural radionuclides initially contained in the ilmenite is finally accumulated in red gypsum (Mantero, et al., 2013).

2.3 Mineral Carbonation of Red Gypsum

Mineral carbonation is a carbon capture and storage (CCS) technique that involves an exothermic chemical reaction. The chemical reaction is the reaction between an oxide containing metals like MgO, CaO, or iron oxides, and carbon dioxide (CO_2) to produce stable solid carbonates such as calcium carbonates ($CaCO_3$), magnesium carbonate ($MgCO_3$) and iron carbonate ($FeCO_3$). One of the proposed techniques for lowering global greenhouse gas (GHG) emissions is the CCS method (Azdarpour, et al., 2014). CCS is one of the possible alternatives for reducing atmospheric CO_2 concentration. In particular, CCS has the potential to provide up to 15% to 55% of the total worldwide climate change mitigation effort by the year 2100 (Riahi, Rubin and Schrattenholzer, 2004). CO_2 is stored in solid form as a stable, which is ecologically friendly mineral carbonate as a result of mineral carbonation. In reality, the procedure is analogous to the natural chemical processes that happen naturally in nature, such as rock weathering over geologic periods.

Mineral carbonates have a lower energy state (60 kJ/mol to 180 kJ/mol) than carbon dioxide CO_2, which has an energy state of 400 kJ/mol. As a result, rather than temporary storage, carbonate sequestration ensures long-term fixing of CO_2 as the products after mineral carbonation is thermodynamically stable (Maroto-Valer, et al., 2005). Many natural minerals have been

examined to use as raw materials for mineral carbonation, for example, olivine, wollastonite, tremolite, serpentine, and some industrial wastes, including waste cement and blast furnace slag. The reason that these mineral materials can be used in mineral carbonation is that they contain vast amounts of primary cations such as calcium ions (Ca^{2+}) and magnesium ions (Mg^{2+}) (Lee, et al., 2012). The feasibility of using another type of gypsum, flue gas desulphurisation (FGD) gypsum, was studied for mineral carbonation by Lee, et al. (2012). According to Lee, et al. (2012), FGD gypsum was suitable for CO_2 sequestration as the carbonation reactivity of FGD gypsum was very high, and the purity of calcium carbonate could be achieved at 90%, as well as the rate of carbonation was achieved at around 95%.

2.3.1 Materials and Equipment Used in Mineral Carbonation

The materials used in the mineral carbonation method are red gypsum, ammonium hydroxide (Na_4OH) and carbon dioxide (CO_2) with a purity of 99.99%, which is shown in Table 2.5 (Azdarpour, et al., 2014). Ammonium hydroxide (Na_4OH) is added to precipitate the metal hydroxides in order to differ in colour and solubility when a qualitative analysis is needed to be performed. For example, Na_4OH reacts with white colour precipitate ferrous carbonate ($FeCO_3$) to form soluble ammonium carbonate ($(Na_4)_2CO_3$) and dirty green precipitate iron hydroxide ($Fe(OH)_2$), which represents in Equation 2.1 (TOPPR, 2022). Figure 2.6 shows the basic equipment used in the mineral carbonation method's experiment and its usage, while Figure 2.5 shows the schematic diagram of the mineral carbonation method.

$$FeCO_3 + Na_4OH \rightarrow (Na_4)_2CO_3 + Fe(OH)_2 \qquad (2.1)$$

Table 2.5: Materials Used and Its Sources (Azdarpour, et al., 2014).

Materials	Sources
Red Gypsum	Landfill of Hutsman Tioxide
Ammonium Hydroxide	Rankem
Carbon Dioxide	Malaysian Oxygen

Table 2.6: Equipment Used and Its Usage.

Equipment	Usage
CO_2 tank	Storage of CO_2
Flow-meter Regulator	Control the flow rate of injected CO_2
High pressure high temperature (HPHT) Autoclave Reactor	The place that reaction occurs
Temperature Controller	Control the temperature of reactor
Magnetic Stirrer	Allow for the homogenisation of mixable liquids
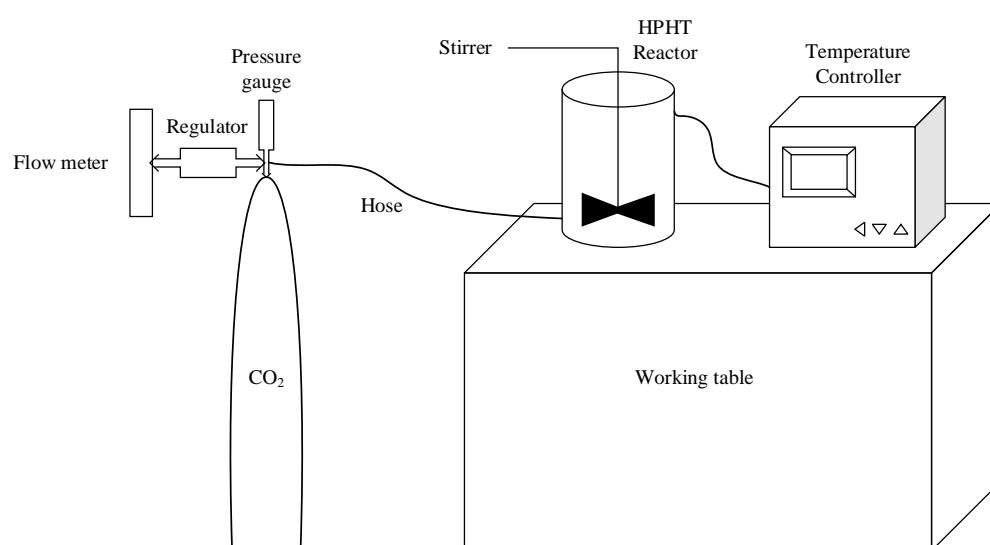
Figure 2.5: Schematic Diagram of Mineral Carbonation Method (Azdarpour et al., 2014; Rahmani, Tyrer and Junin, 2014).

2.3.2   Parameters Study in Mineral Carbonation

There are three important parameters investigated in mineral carbonation in order to achieve the most effective separation of red gypsum: particle size of red gypsum, the pressure of CO_2 and reaction temperature. According to Azdarpour, et al. (2014), the smaller the particle size of red gypsum, the higher the carbonation efficiency. It is because the overall surface area of the smaller particles is greater than that of the larger particles. The total specific surface area of red gypsum particle plays a role in determining the overall conversion rate of calcium and iron into their carbonate state (Huijgen, Witkamp and

Comans, 2006; Kakizawa, Yamasaki and Yanagisawa, 2001; Park and Fan, 2004). In the research of O'Connor, et al. (2001), they concluded that the conversion of Mg ions was increased from 10% to 90% when the particle size was reduced from 106 – 150 μm to roughly 37 μm. Besides, Kodama, et al. (2008) also supported this point of view with their research which showed that the particle size of steel slag was a significant parameter controlling the conversion of Ca into $CaCO_3$, with the minimum particle size of 63 μm and achieved 60% efficiency. Figure 2.6 shows the influence of particle size of RG on carbonation efficiency.
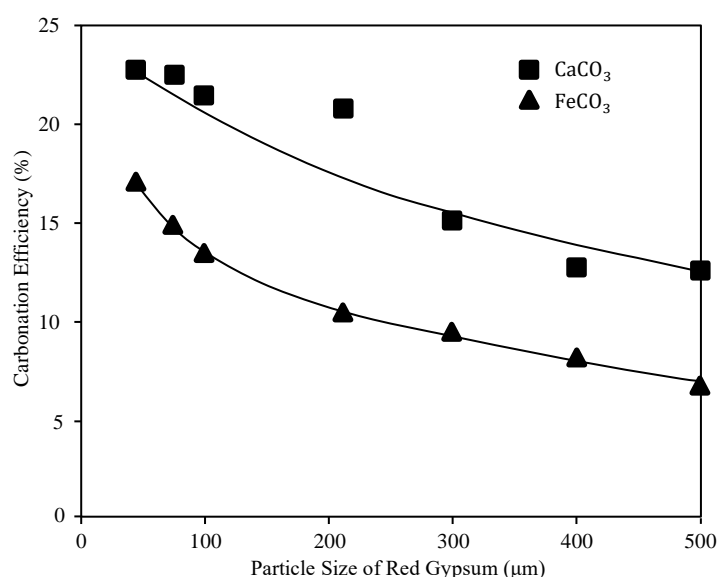
Figure 2.6: Influence of Particle Size of RG on Carbonation Efficiency
(Azdarpour, et al., 2014).

In the mineral carbonation method, when the pressure of CO_2 was increased from 1 bar to 70 bar, the carbonation efficiency was also increased (Azdarpour, et al., 2014). The concentration of HCO_3^- and CO_3^{2-} ions in solution substantially impacts the carbonate precipitation. According to Henry's Law, the concentration of carbonic acid solution H_2CO_3 is proportional to the partial pressure of CO_2. As a result, higher CO_2 pressure appears to encourage an increase in calcium and iron ion precipitation. However, increasing CO_2 pressure produces only a little amount of CO_3^{2-}. Since the CO_3^{2-} ion concentration is deficient in that scenario, a very high metal ion concentration is necessary to precipitate metal carbonate (Chen,

O'Connor and Gerdemann, 2006). Furthermore, increasing the pressure of CO_2 lowers pH of the solution, which aids in the extraction of calcium and iron from red gypsum. It can also be concluded that lowering pH aids the leaching of metal ions from metal silicate, but it also reduces CO_3^{2-} concentration (Chen, O'Connor and Gerdemann, 2006; Herk, Pietersen and Schuiling, 1989). As a result, these findings point to a delicate balance in improving Fe extraction from red gypsum while also promoting precipitation of carbonate. Furthermore, Gerdemann, et al., (2007) stated that increasing the pressure of CO_2 will accelerate CO_2 dissolution and improve its carbonation kinetics, resulting in the reaction being forwarded. Figure 2.7 shows the influence of the pressure of CO_2 on carbonation efficiency.
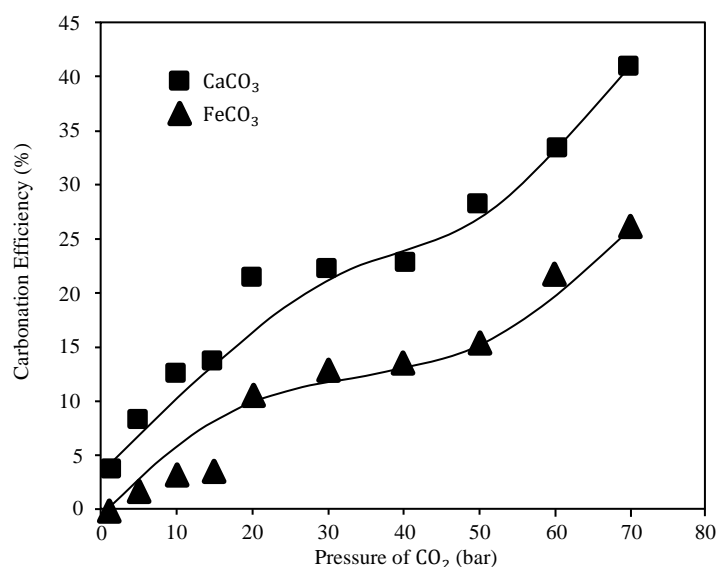
Figure 2.7: Influence of Pressure of CO_2 on Carbonation Efficiency
(Azdarpour, et al., 2014).

In the research of Azdarpour, et al. (2014), carbonation efficiency is increased when the temperature is increased from ambient temperature up to 200 °C, while it will decrease with the further increment of the temperature. Above statement was also supported by the research of Chen, O'Connor and Gerdemann (2006). They concluded that increasing the temperature of the reaction enabled easier extraction of the metal ions from the feedstock, which has a huge impact on precipitation of carbonate. Temperature affects Henry's constant (K_H), carbonate solubility product (K_{sp}), and first- and second-order

dissociation of carbonic acid (K_{a1} and K_{a2}). The K_H value increases as the reaction temperature increases, reducing the amount of CO_2 gas in the solution. Increasing the reaction temperature causes the value of K_{sp} becomes lower, resulting in the precipitation of metal ions being more easily happening at higher temperatures than ambient temperatures. Finally, as temperature increases, the value of K_{a1} and K_{a2} increases as well, indicating that more CO_2 creates bicarbonate ions, which then change to carbonate ions at higher temperatures. Temperature increases K_{a1} and K_{a2} while decreases K_{sp}, allowing carbonates to precipitate more easily. Since the competing effects which the greater K_H has the opposite effect, therefore there should be an optimum temperature for this reaction. Figure 2.8 shows the influence of temperature on carbonation efficiency.
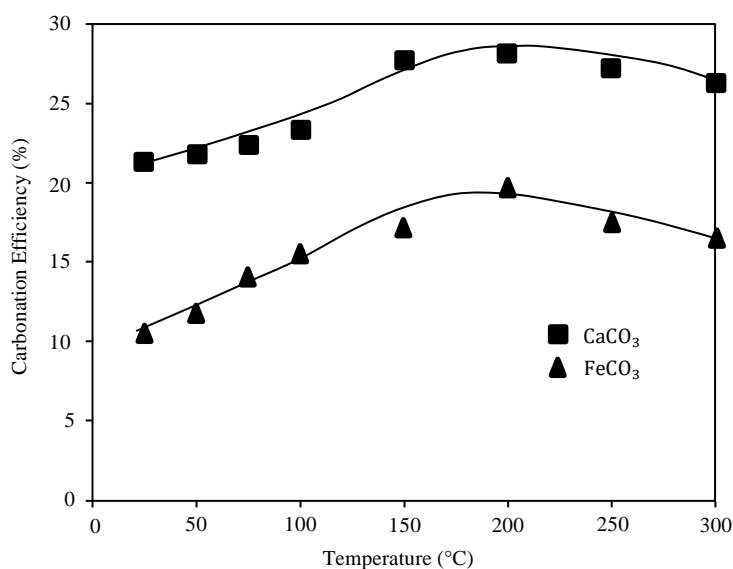
Figure 2.8: Influence of Temperature on Carbonation Efficiency (Azdarpour, et al., 2014).

2.3.3   Feasibility Study of Carbonation Method

Azdarpour, et al. (2014) conducted an experiment to study the feasibility of RG for mineral carbonation with several parameters, including particle size of red gypsum, CO_2 pressure, and reaction temperature which explained earlier. The study was conducted since RG contains large amounts of iron and calcium ions, so the $FeCO_3$ and $CaCO_3$ can be produced through the mineral carbonation process. Thus, the purpose which the extraction of iron from RG

is also achieved. Equation 2.2 is used to calculate both carbonates' purities. Equations 2.3 and 2.4 are used to calculate the metal content inside the RG and the carbonation efficiency.

$$P_{XCO_3}(\%) = \frac{\Delta W(\%) \times MW_{XCO_3}}{MW_{CO_2}} \tag{2.2}$$

$$X \text{ mass in } XCO_3 = \frac{\Delta W(\%) \times MW_X \times \text{mass of solid residue}}{MW_{CO_2}} \tag{2.3}$$

$$\text{Carbonation efficiency } (\%) = \frac{X \text{ mass in } XCO_3 - X \text{ mass in reaction mixture}}{X \text{ total mass in reaction mixture}} \times 100 \tag{2.4}$$

where

P_{XCO_3} = purity of product, %

X = iron or calcium in red gypsum

ΔW = weight loss of sample, kg

MW_X = molecular weight of iron or calcium, g/mol

The chemical reactions of both iron hydroxide ($Fe(OH)_2$) and calcium sulphate ($CaSO_4$) are illustrated in Equations 2.5 and 2.6 (Rahmani, Tyrer and Junin, 2014). After Azdarpour, et al. (2014) conducted the experiment, mineral carbonation of RG could significantly produce calcium carbonate. However, the extraction rate of iron metal was low, and the highest efficiency in the entire experiment was about 26.31% for iron extraction. Therefore, it is not suitable for this study as the extraction rate of iron is low and the product will be challenging to reutilise in other applications. Although this method is not suitable, this innovative technology is appealing and environmentally friendly since it can address two environmental issues: reutilising hazardous industrial waste (red gypsum) and reducing GHG emissions. However, low product's purity and carbonation efficiency remain significant challenges.

$$Fe(OH)_2 + CO_2 \rightarrow FeCO_3 + H_2O \tag{2.5}$$

$$CaSO_4 + CO_2 + H_2O \rightarrow H_2SO_4 + CaCO_3 \tag{2.6}$$
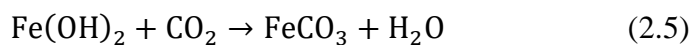
2.4 Acid Leaching Method

Leaching is one of the standard separation processes for solid-liquid extraction. This method is used to eliminate the unwanted solute constituent from the multicomponent solid-phase based on the differences in solubility in the solvent. When the multicomponent solid is contacted with the liquid phase solvent, the undesired solute or desired solute will diffuse from the multicomponent solid to the solvent. As a result, the desired solute components can be obtained (Geankoplis, Hersel and Lepek, 2018). In this study, red gypsum is considered as the multicomponent solid phase, which needs to eliminate the iron metal (an unwanted solute constituent) and leave the natural gypsum (desired solute component) in the original solid phase in contact with the acid or base (solvent).

According to Blencoe, et al. (2014), serpentine, one of the minerals, dissolves slowly and requires a long time in an alkaline solution when extracting components from serpentine, so alkaline solutions are ineffective to use as a solvent to extract minerals. Using serpentine as a reference is because iron metal is the common ion present in both red gypsum and serpentine. Azdarpour, et al. (2015) further proved that alkaline solutions were ineffective in leaching by conducting an experiment to extract iron and calcium metals from the RG. It was found that when sodium hydroxide (NaOH) and potassium hydroxide (KOH) with a concentration from 0.1 M up to 4 M were used as a solvent to extract iron and calcium from RG, there was no calcium and iron were extracted. Another alkaline solution, ammonium hydroxide (Na_4OH) was used to replace NaOH and KOH. However, the result was similar to the NaOH and KOH solutions which the extraction rate of calcium and iron was 0.3% and 0.1%, respectively. This experiment was conducted under the condition which the temperature of reaction of 25 °C and the reaction time of 60 minutes. Therefore, more residence time is needed in order to improve the extraction rate of calcium and iron in the alkaline solutions. As a result, alkaline solutions are ineffective extracting agents or solvents to extract the metals from RG (Azdarpour, et al., 2015). Thus, alkaline solutions as extracting agents are not being discussed in this study.

2.4.1 Extraction Efficiency of Different Acids

Aside from alkaline solutions, Azdarpour, et al. (2015) also conducted an experiment which used acids in the leaching process. Compared to alkaline solutions, acids are more suitable for extracting iron and calcium from the RG. Under the same condition with alkaline leaching previously, three acids were used to analyse the best extraction efficiency, which were sulphuric acid (H_2SO_4), hydrochloric acid (HCl) and nitric acid (HNO_3). The results showed that by using 4 M of H_2SO_4 as extracting agents, the extraction rate of iron metal is the highest, which is 19.7%, while by using 4 M of HCl and 4 M of HNO_3, the extraction rate of iron metal is only 18.8% and 13.1%, respectively. Therefore, the H_2SO_4 extracting agent has the highest extraction efficiency in leaching of RG, followed by HCl and HNO_3.

According to Azdarpour, et al. (2015), 2 M of H_2SO_4, HCl and HNO_3 extracted 84.6%, 73.5% and 54.9% of Fe from RG at 70 °C of reaction temperature and reaction time of 120 minutes. From this, it can be further explained that H_2SO_4 has the highest ability to extract iron metal from red gypsum for the same concentration with different reaction temperatures and times. The results are in agreement with the results of Teir, et al. (2007), which the most effective acid for extracting iron from natural serpentine is H_2SO_4, followed by HCl, HNO_3, HCOOH and CH_3COOH.

2.4.2 Mechanism of Iron Oxide Leaching

As discussed in **Section 1.1**, ilmenite ore (mainly consisting of $FeTiO_3$) reacts with H_2SO_4 to produce $FeSO_4$ before being oxidised to $Fe_2(SO_4)_3$. Both $FeSO_4$ and $Fe_2(SO_4)_3$ are unstable under condition circumstances and undergo hydrolysis to form $Fe(OH)_2$ and $Fe(OH)_3$ when the pH value is in the range of 3 to 6. $Fe(OH)_2$ can be further oxidised into $Fe(OH)_3$. In the acid leaching process, $Fe(OH)_3$ reacts with H_2SO_4 which is a neutralisation reaction to produce $Fe_2(SO_4)_3$ which is soluble in water. As a result, the purpose of separating and extracting iron oxide can be achieved. The schematic mechanism of iron oxide leaching is shown in Figure 2.9 and Equation 2.7 (Jiang, Sun and Peng, 2019).

$$2Fe(OH)_3 + 3H_2SO_4 \rightarrow Fe_2(SO_4)_3 + 6H_2O \qquad (2.7)$$
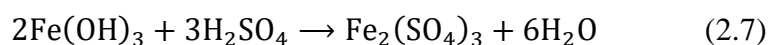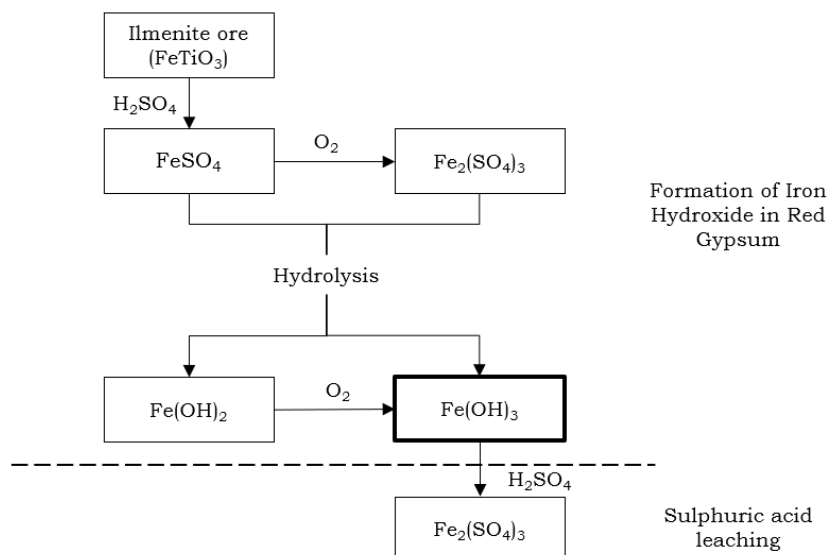
Figure 2.9: Schematic Diagram of the Sulphuric Acid Leaching Method (Jiang, Sun and Peng, 2019).

2.4.3 Materials and Equipment Used in Acid Leaching Method

The materials used in the sulphuric acid leaching method are red gypsum and sulphuric acid (H_2SO_4) with purity greater than 95%, as shown in Table 2.7 (Azdarpour, et al., 2015). Table 2.8 shows the basic equipment used in the sulphuric acid leaching method's experiment and its usage, while Figure 2.10 shows the schematic diagram of the sulphuric acid leaching method.

Table 2.7: Materials Used and Its Usage (Azdarpour, et al., 2015).

Materials	Usage
Red Gypsum	To synthesis natural gypsum for reutilise in other applications.
Sulphuric Acid, H_2SO_4	To act as extracting agent and remove iron metal in red gypsum.

Table 2.8: Equipment Used and Its Usage.

Equipment	Usage
Water bath	Keeps samples at a steady temperature for an extensive period
Glass Reactor	The place that reaction occurs
Temperature Controller	Control the temperature of reactor
Magnetic Stirrer	Allow for the homogenisation of mixable liquids
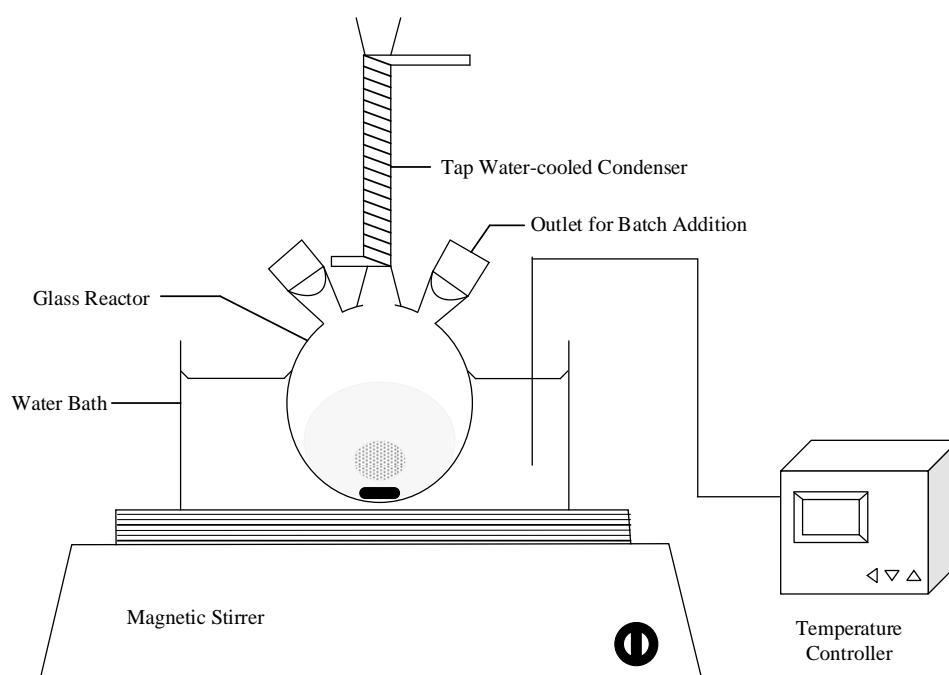
Figure 2.10: Schematic Diagram of the Sulphuric Acid Leaching Method (Azdarpour, et al., 2015).

2.4.4 Parameters Study in Acid Leaching Method

There are five important parameters investigated in sulphuric acid leaching in order to achieve the most effective separation of red gypsum: the concentration of H_2SO_4, solid-liquid ratio (S/L ratio), reaction time, reaction temperature and particle size of red gypsum. As discussed in **Section 2.4.2**, H_2SO_4 will undergo a neutralisation reaction with RG, producing $Fe_2(SO_4)_3$ which is soluble in water to extract the iron from RG. Therefore, the increased concentration of H_2SO_4 will produce more $Fe_2(SO_4)_3$. When the extraction rate of iron is increased until the critical point, the iron hydroxide

concentration in the RG has limited the extraction rate of iron as the concentration of iron hydroxide in RG is constant. Thus, when the concentration of H_2SO_4 increases until sufficient to react with the iron hydroxide fully, continue increasing the concentration of H_2SO_4 will no longer increase the extraction rate of iron.

Figure 2.11 shows the graph of the extraction rate against the concentration of sulphuric acid (Jiang, Sun and Peng, 2019). According to Azdarpour, et al., (2015), only 1.3% of iron can be extracted using 0.1 M of H_2SO_4 under ambient temperature in 1 hour. However, using 4 M of H_2SO_4 can achieve an extraction rate of 19.7%, which indicates that the higher the concentration of H_2SO_4, the higher the extraction rate of iron until the critical point is reached.
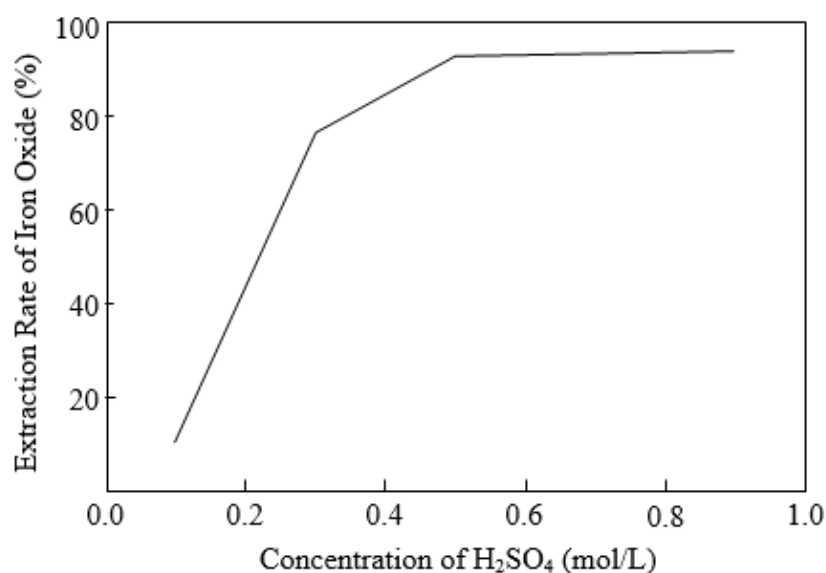
Figure 2.11: Extraction of Iron Oxide versus Concentration of H_2SO_4 (Jiang, Sun and Peng, 2019).

As the solid-liquid ratio decreases within a specific range, the volume of $H_2SO_4 – H_2O$ distributed per unit mass of red gypsum increases, which is more conducive to the dissolution of iron oxide until reaching the critical point. When all soluble iron oxide has been dissolved, continue reducing the solid-liquid ratio, and the iron extraction rate will no longer be increased. When 1:5 g/mL of solid-liquid ratio was used, the iron extraction rate was only 46.38%. The extraction rate of iron is increased to 88.54% at a solid-liquid ratio of 1:10

g/mL, while the extraction rate of iron is increased to 92.83% at a solid-liquid ratio of 1:12.5 g/mL. Besides, when the solid-liquid continues decreasing to 1:15 g/mL and 1:17.5 g/mL, the extraction rate of iron remains at 92.83%, which means the critical point was reached at the solid-liquid ratio of 1:12.5 g/mL. Figure 2.12 shows the graph of the extraction rate against the solid-liquid ratio (Jiang, Sun and Peng, 2019). This indicates that the higher the reaction time in the system, the higher the extraction rate of iron until the critical point is reached.
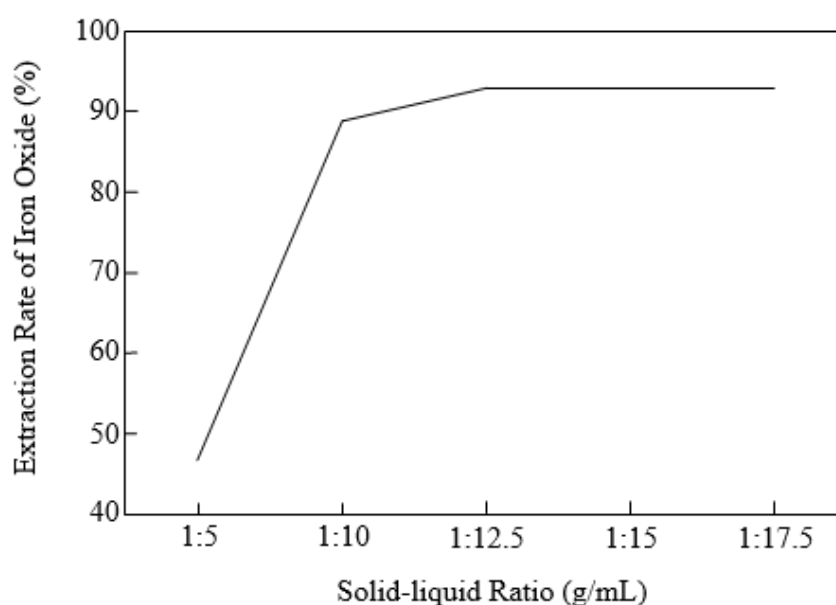
Figure 2.12: Extraction of Iron Oxide versus Solid-liquid Ratio (Jiang, Sun and Peng, 2019).

In the acid leaching process, the solute, iron oxide or iron hydroxide diffuse from red gypsum into the solvent, sulphuric acid. Therefore, more solutes can diffuse into the solvent when the reaction time is longer. According to Azdarpour, et al., (2015), 55.77% of iron can be extracted in 30 minutes by using 2 M of H_2SO_4. The extraction rate of iron is increased to 69.43%, 78.37% and 84.6% at a reaction time of 60 minutes, 90 minutes and 120 minutes, respectively. This indicates that the higher the reaction time in the system, the higher the extraction rate of iron until the critical point is reached. Figure 2.13 shows the graph of extraction rate against reaction time, according to Jiang, Sun and Peng (2019).
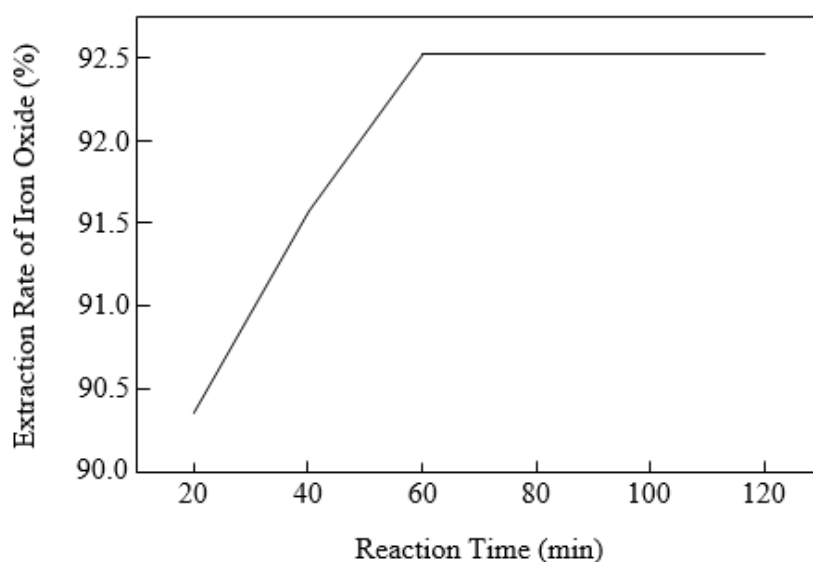
Figure 2.13: Extraction of Iron Oxide versus Reaction Time (Jiang, Sun and Peng, 2019).

When the reaction temperature is low, the number of molecules that reach the lowest activation energy in the reaction system is less, so less iron oxide in RG can react with sulphuric acid. Eventually, the extraction rate of iron is lower. As the temperature of the reaction system increases, the number of activated molecules in the system is increased. Therefore, the extraction rate of iron oxide increases with the increase of the reaction temperature. Figure 2.14 shows the graph of extraction rate against reaction temperature (Jiang, Sun and Peng, 2019). According Azdarpour, et al., (2015), 23.6% of iron can be extracted at 30 °C by using 2 M of H_2SO_4. The extraction rate of iron is increased to 41.8% and 84.6% at the reaction temperature of 50 °C and 70 °C, respectively. This indicates that the higher the reaction temperature in the system, the higher the extraction rate of iron until the critical point is reached.
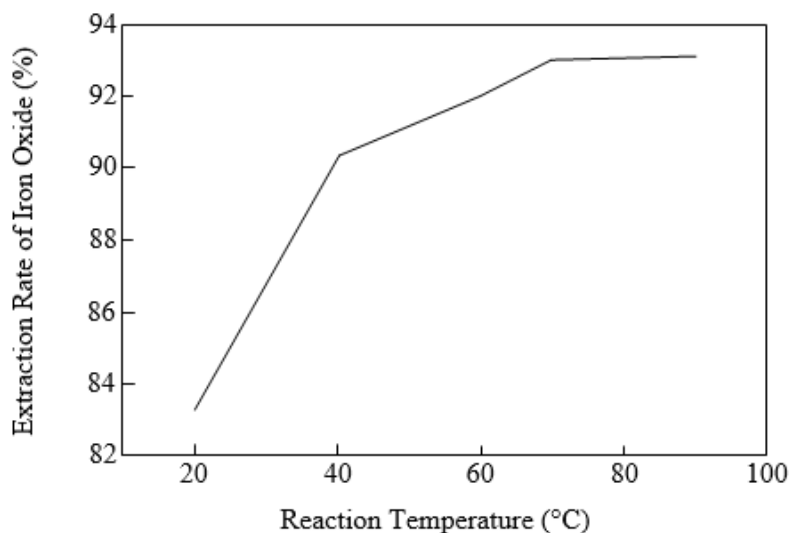
Figure 2.14: Extraction of Iron Oxide versus Reaction Temperature (Jiang, Sun and Peng, 2019).

O'Connor, et al. (2001) found that reducing particle size from 150 μm to roughly 37 μm can increase the Mg ions conversion from 10% to 90%. Besides, Kodama, et al. (2008) concluded that the particle size of steel slag is a significant parameter controlling the calcium conversion into calcium carbonate. Calcium conversion into calcium carbonate can be improved with the smallest particle size of steel slag. Furthermore, Azdarpour, et al., (2014) concluded that the extraction rate of iron increases when decreasing the particle size of red gypsum in the mineral carbonation of red gypsum. Based on this research, particle size is one of the crucial parameters that will affect the extraction rate of iron from RG. It is because RG has a larger total surface area when its particle size is smaller, so more RG can contact the sulphuric acid. Thus, the extraction rate can be increased.

2.4.5   Phase Transformation of Red Gypsum in Acid Leaching Products
There are a total of three different phases of gypsum involved in the acid leaching process, which include anhydrous (AH) gypsum ($CaSO_4$), hemihydrate (HH) gypsum, ($CaSO_4 \cdot 0.5H_2O$) and dihydrate (DH) gypsum ($CaSO_4 \cdot 2H_2O$). The structure of DH gypsum is formed by the combination of Ca^{2+}, SO_4^{2-} and H_2O to form a structural layer. Hydrogen bonds formed by H_2O molecules connect the structural layers. The position between structural

layers, which is parallel to the (010) plane, is the weak point in the structure. During the acid leaching process, the H_2O molecules coordinated with Ca^{2+} can be eliminated along with the weak points of the structural layers, and the Ca^{2+} and SO_4^{2-} shifted restructuring accordingly. With the changes in sulphuric acid concentration, solid-liquid ratio, reaction time and reaction temperature, DH gypsum is gradually dehydrated under solid-phase conditions and undergoes structural adjustment to transform into HH gypsum and/or AH gypsum. Equations 2.8 to 2.10 illustrate the transformation of DH gypsum into HH gypsum and/or AH gypsum (Jiang, Sun and Peng, 2019).

$$CaSO_4 \cdot 2H_2O \rightarrow CaSO_4 \cdot 0.5H_2O + 1.5H_2O \qquad (2.8)$$
$$CaSO_4 \cdot 2H_2O \rightarrow CaSO_4 + 2H_2O \qquad (2.9)$$
$$CaSO_4 \cdot 0.5H_2O \rightarrow CaSO_4 + 0.5H_2O \qquad (2.10)$$
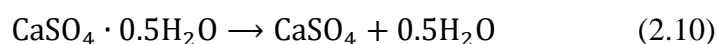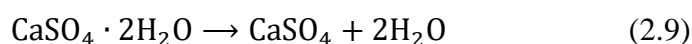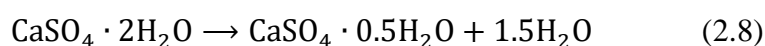
2.4.6   Feasibility Study of Acid Leaching

According to Azdarpour, et al. (2015), the extraction rate of iron can achieve 84.6% by using H_2SO_4 as solvent under conditions at 70 °C of reaction temperature, the reaction time of 120 minutes and the concentration of H_2SO_4 is 2 M. Besides, Jiang, Sun and Peng (2019) showed that the extraction rate of iron could up to 93.14%, at the same time, the concentration of H_2SO_4 and reaction time can decrease to 0.5 M and 60 minutes respectively, when the solid-liquid ratio of 1:12.5 is considered.

The Fourier Transform Infrared Spectroscopy (FTIR) results can further support the results. The FTIR analysis of solid residues after acid leaching of red gypsum with 2 M sulphuric acid at a temperature of 70 °C and reaction time of 120 minutes is shown in Figure 2.15. Six peaks are clearly seen in Figure 2.15, such as 3220, 1720, 1091, 1015, 667 and 583, which indicate $O - H$, $Al - O$, SO_4^{2-}, $Si - O$, SO_4^{2-}, $Fe - O$, respectively. The $Fe - O$ bonds in the solid residues indicate that the sulphuric acid leaching process cannot extract all the iron metal from RG (Azdarpour, et al., 2015).
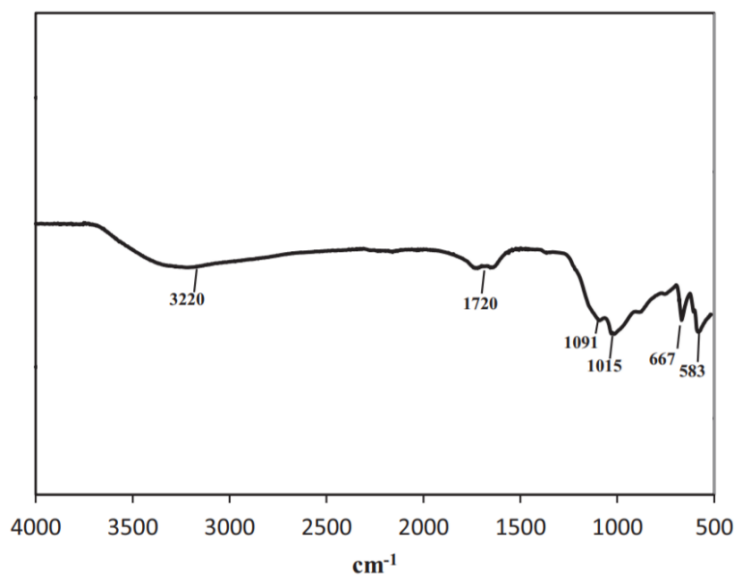
Figure 2.15: FTIR Analysis of Solid Residue after Acid Leaching of RG
(Azdarpour, et al., 2015).

On the other hand, Figure 2.16 shows the surface morphologies and microstructures of products after acid leaching. The iron oxides in the form of fine particles or aggregates have disappeared compared to Figure 2.3, indicating that the sulphuric acid leaching method can effectively extract and separate iron from red gypsum. It also increases the purity of gypsum products (Jiang, Sun and Peng, 2019).
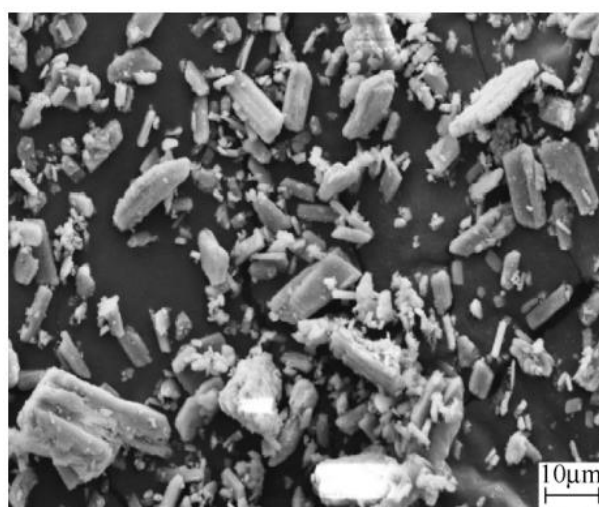
Figure 2.16: SEM Image of Acid Leaching Products of Red Gypsum (Jiang, Sun and Peng, 2019).

In a nutshell, using acid (H_2SO_4) leaching to pretreat red gypsum is significantly effective in separating iron metal and improving the purity and whiteness of products after the acid leaching process. The purity and whiteness of the products can achieve 97% and 54.4, respectively, which means the products are easier to reutilise in other applications. Besides, this acid leaching method has a simple technological process for extracting iron metal and has low equipment requirements. Furthermore, the produced acidic filtrate containing $Fe_2(SO_4)_3$ can be recycled. When $Fe_2(SO_4)_3$ is nearly saturated, calcium oxide or calcium hydroxide can be used to carry out neutralisation treatment, adjusting pH in a range of 3.5 to 4.5 in order to precipitate $Fe(OH)_3$. Finally, the acidic waste liquid produced after filtration and separation can be recycled. (Jiang, Sun and Peng, 2019).

2.5   Hydrothermal Treatment Method

Hydrothermal treatment (HTT) is a crystal synthesis technique that relies on the mineral's solubility in hot water under high-pressure circumstances (Pan, et al., 2015). According to Peng, et al. (2021), two main factors affect iron removal efficiency, including the characteristics of the solid phases and the iron speciation. Most research has failed to efficiently extract iron from red gypsum because of the lack of understanding and control over solid phase microstructure and iron speciation.

More evidences that the properties of solid phases and heavy metal speciation are essential in removing heavy metal from solid wastes under HTT is supported by Liu, et al. (2019) and Liu, et al. (2018). Liu, et al. (2019) stated that the heavy metals adsorbed on the particles' surface could be effectively recovered from solid wastes under hydrothermal conditions with well controlling the transformation of phase. Besides, Liu, et al. (2018) also showed that the chromium Cr(VI) ions could be fully recovered from the gypsum sludge that contains hazardous Cr(VI) under hydrothermal conditions with well controlling the transformation of phase.

2.5.1　Mineraliser

Mineralisers were often used in the hydrothermal treatment, and it was used to increase the rate of crystal growth and control the heavy metals' speciation. Persulfate salts were used as mineraliser in the study conducted by Liu, et al. (2018) to release the CrO_4^{2-} incorporated in hazardous Cr(VI)-containing gypsum sludge and transform CrO_4^{2-} into $Cr_2O_7^{2-}$ species which it has less binding energy to gypsum, leading to fully extraction of Cr(VI) from the hazardous Cr(VI)-containing gypsum sludge with a very high efficiency which more than 99.5%.

Peng, et al. (2021) conducted an experiment that used HTT without mineraliser to extract the iron metal from RG. However, only about 3% of iron was extracted from RG, and the products were still dark red (21.9 of whiteness), indicating there is still a lot of iron metal inside the gypsum. This method failed to extract iron from RG efficiently because the mineraliser was not added to the experiment. Through the experiment conducted by Liu, et al. (2018), the role of mineraliser is vital as it is used to regulate the speciation of heavy metals and increase the rate of crystal growth, which can improve the extraction rate of heavy metals. Besides, hydrogen ion (H^+) was the most critical factor of the mineralisers in extracting Cr(VI) from hazardous Cr(VI)-containing gypsum to the supernatant under HTT. When H^+ concentration increased, the crystal growth rate was increased, and the phase transformation of gypsum was reduced, which is favourable for improving the extraction efficiency of Cr(VI) (Zheng, et al., 2019).

Peng, et al. (2021) conducted another experiment that included acid mineraliser in the HTT. Using 1.0 M and 1.5 M HCl as the mineraliser, the efficiency of iron extraction was achieved at 49.2% and 99.2%, respectively. The whiteness of the products was reached 87.8, and the occurrence of products was white. Figure 2.17 and Figure 2.18 show the comparison between the efficiency of iron extraction and whiteness of HTT with acid and without acid. It is clearly to be seen that the removal effectiveness of iron after HTT with acid was 30 times higher than that after HTT without acid. Therefore, it can be concluded that in order to completely remove iron and improve the whiteness of solid products, both hydrothermal treatment and acid mineraliser are required.
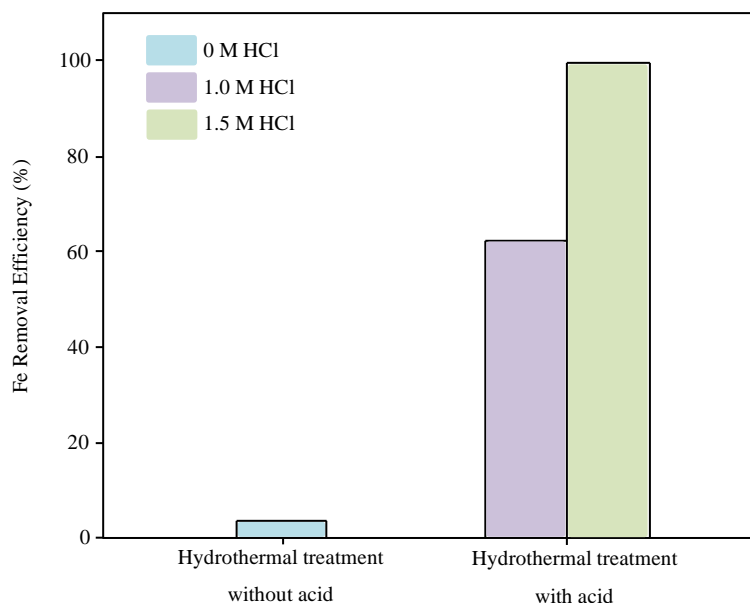
Figure 2.17: The Comparison between The Efficiency of Iron Extraction of
HTT with and without Acid (Peng, et al., 2021).
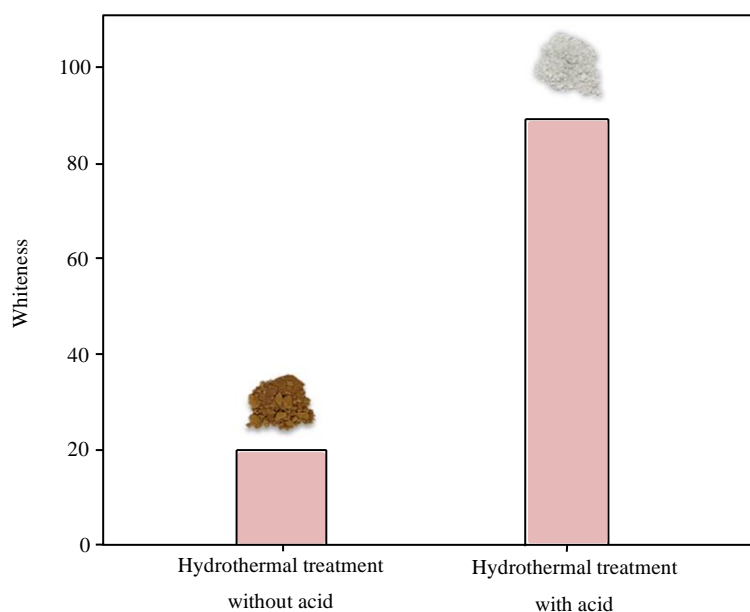
Figure 2.18: The Comparison between The Whiteness of HTT with and
without Acid (Peng, et al., 2021).

2.5.2   Materials and Equipment Used in Hydrothermal Treatment

The materials used in the hydrothermal treatment method are red gypsum,
deionized water and hydrochloric acid (HCl) with purity greater than 95%,
shown in Table 2.9 (Peng, et al., 2021). Table 2.10 shows the basic equipment
used in the hydrothermal treatment method's experiment and its usage, while

Figure 2.19 shows the schematic diagram of the hydrothermal treatment method.

Table 2.9: Materials Used and Its Usage (Peng, et al., 2021).

Materials	Usage	Sources
Red Gypsum	To synthesis natural gypsum for reutilise in other applications.	Sichuan Province, China
Deionized Water	To break down the particles.	-
Hydrochloric Acid, HCl	To act as mineraliser in hydrothermal conditions.	Guangzhou Chemical Reagent Factory

Table 2.10: Equipment Used and Its Usage.

Equipment	Usage
Teflon Container	To contain the mineraliser, deionized water and red gypsum.
Hydrothermal Autoclave Reactors	The place that reaction occurs
Temperature Controller	Control the temperature of reactor
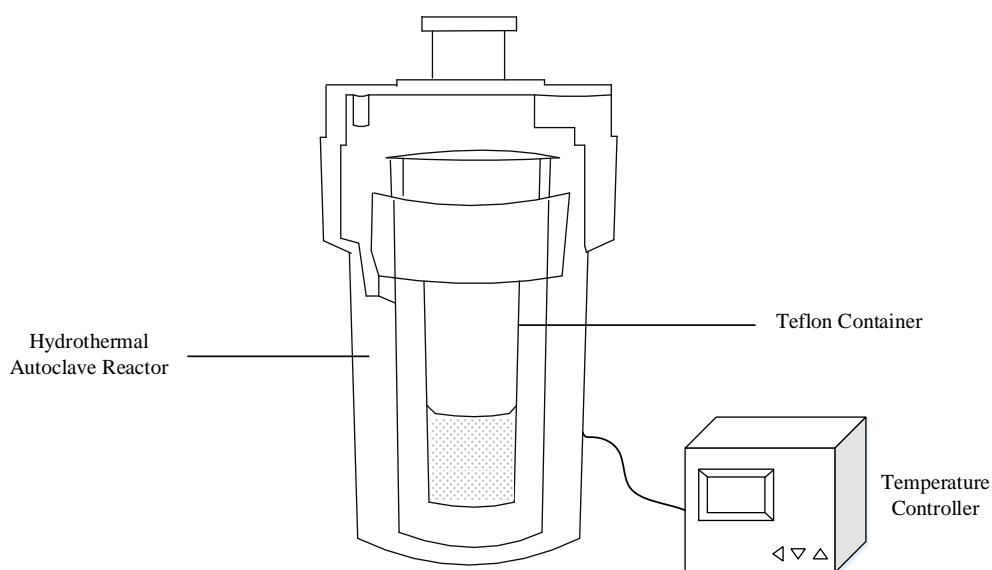
Figure 2.19: Schematic Diagram of the Hydrothermal Treatment Method
(Peng, et al., 2021).

2.5.3 Parameters Study in Hydrothermal Treatment

There are four important parameters investigated in hydrothermal treatment similar to the sulphuric acid leaching method to achieve the most effective separation of red gypsum: liquid-solid ratio (L/S ratio), heating time, heating temperature and concentration of HCl. The reason for investigating the parameters, L/S ratio, heating time and temperature are discussed in **Section 2.4.4.** The removal efficiency of iron rose as the L/S ratio increased, as illustrated in Figure 2.20. When the L/S ratio was 6 or 8, the iron removal efficiency was less than 80%. It achieved the optimal when the L/S ratio was 10, the iron removal efficiency was higher than 99%. Besides, the optimum heating temperature and time is at 140 °C and 6 h as shown in Figure 2.21 and Figure 2.22, respectively. At the same time, as illustrated in Figure 2.21, it can be clearly seen that 1.5 M HCl has the best efficiency of iron extraction among 0.5 M, 1.0 M and 1.5 M HCl. The theory behind how the concentration of mineraliser affects the efficiency will be discussed in **Section 2.5.4**.
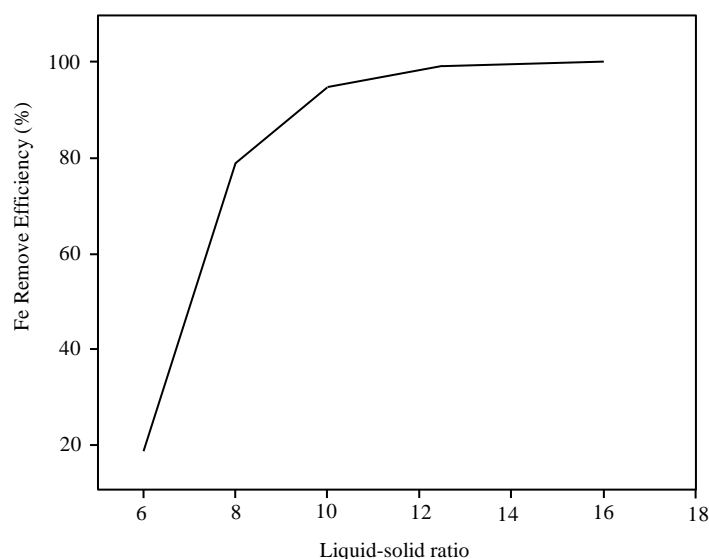
Figure 2.20: Removal Efficiency of Iron versus Liquid-solid Ratio (Peng, et al., 2021).
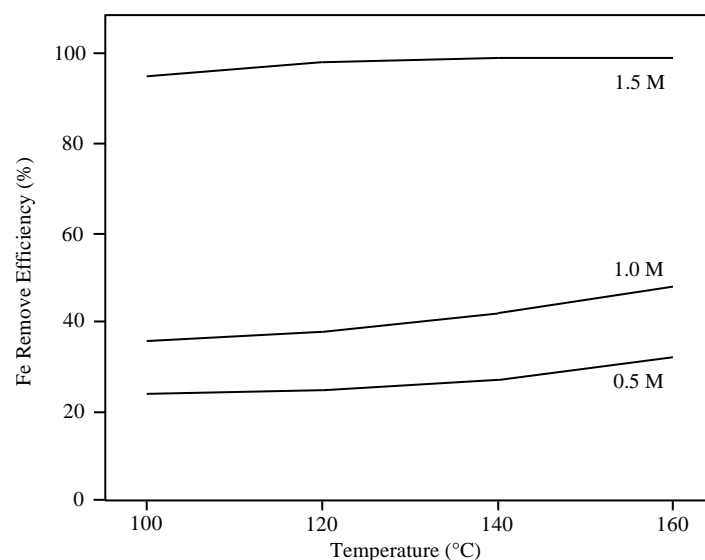
Figure 2.21: Removal Efficiency of Iron versus Temperature and HCl
concentration (Peng, et al., 2021).
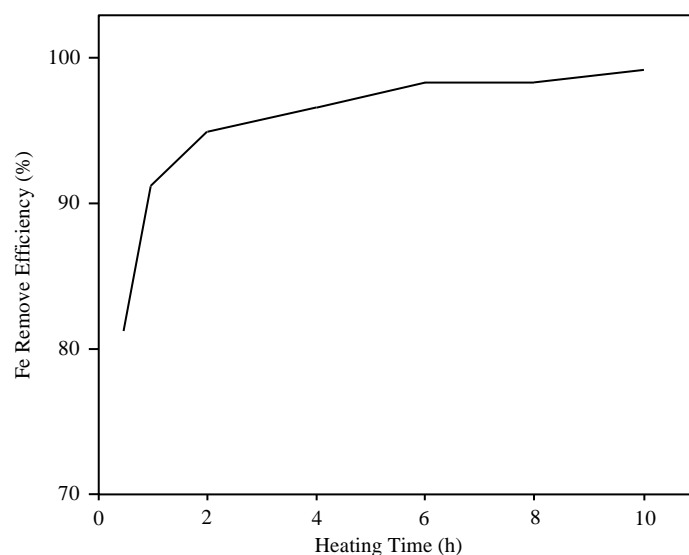
Figure 2.22: Removal Efficiency of Iron versus Heating Time (Peng, et al.,
2021).

2.5.4   Iron Speciation

Iron speciation is discussed in this section to review the different phases
(insoluble or soluble) of different redox species in different pH values. As
mentioned in **Section 2.5**, iron speciation is one factor that affects the
efficiency of extracting iron from RG. **Section 2.5.1**, mentioned that the
efficiency of iron removal was increased when the concentration of HCl
increased. It indicates that iron removal's efficiency depends on the

supernatant's pH value. When the supernatant's pH value decreases, iron removal efficiency drastically increases. When the pH value is greater than 4, iron removal efficiency is dropped to less than 30%. In comparison, the efficiency of iron removal increased to approximately 90% when the pH value of the supernatant was less than 1. Figure 2.23 shows the graph of removal efficiency of iron against to supernatant's pH value (Peng, et al., 2021).
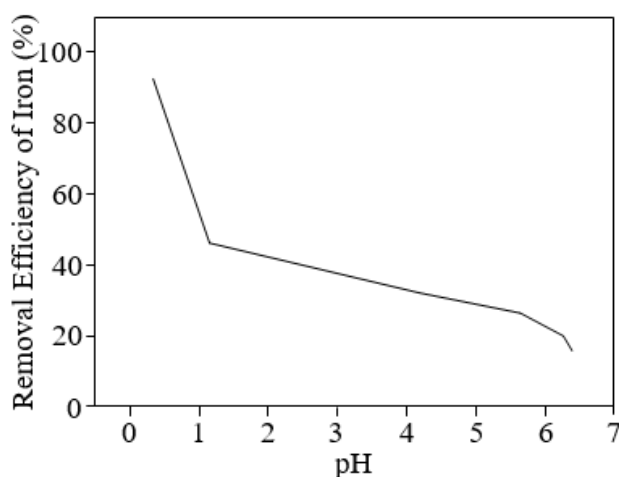
Figure 2.23: Removal Efficiency of Iron Against to Supernatant's pH Value (Peng, et al., 2021).

Besides, when the pH value of supernatant is greater than 1, iron hydrolysis occurs, and the insoluble compounds, including lepidocrocite and colloidal ferric hydroxide, are formed by hydrolysates such as $Fe(OH)_2^+$, $Fe(OH)_4^-$ and $FeOH^{2+}$ (Liu and Millero, 2002; Stefánsson, 2007). When 1.5 M HCl is used as mineraliser under HTT conditions, the pH value of the supernatant is less than 1. Therefore, soluble Fe^{3+} is formed from the insoluble ferric hydroxides, Fe^{3+} is then dissolved into the supernatant and removed by filtration. Figure 2.24 shows the graph of iron species versus pH value at $[Fe]_{tot} = 0.793$ mmol (Peng, et al., 2021).
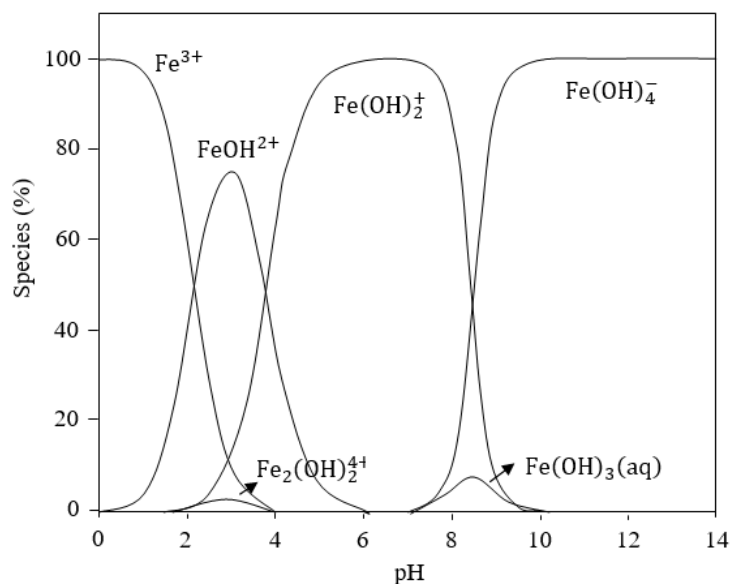
Figure 2.24: Iron Species versus pH Value at $[Fe]_{tot} = 0.793$ mmol (Peng, et al., 2021).

This can support by Zheng, et al., (2019) and Ma, et al., (2020). In the hydrothermal treatment of chromium-containing gypsum waste, Zheng, et al., (2019) discovered that H^+ was a significant role in lowering the temperature of phase transformation of chromium-containing gypsum and accelerating crystal growth, resulting in total extraction (99.8%) of Cr(VI) from chromium-containing gypsum. Besides, arsenic- and trace metals-bearing gypsum was successfully extracted more than 99.9% of arsenic and 90% of other trace elements (Me^{2+}), such as Cu^{2+}, Zn^{2+}, Pb^{2+}, and Cd^{2+}, with $HAsO_4^{2+}/Me^{2+}$ converted into H_3AsO_4 / $MeCl_n^{(2-n)}, (1 \leq n \leq 4)$ by hydrothermal recrystallization (Ma, et al., 2020).

2.5.5 Mechanism of Iron Removal

In water, the crystalline phase of RG which is $CaCO_3$ and HH gypsum, is first transformed into the DH gypsum phase. In the meantime, a portion of amorphous iron oxide or hydroxide converts to soluble Fe^{3+} ions in the presence of an acid, which is released into the solution, resulting in partial iron extraction. On the other hand, the DH particles retained their rough surface, irregular form and aggregated state, causing iron adsorption or incorporation. Furthermore, the phase transformation from DH gypsum to AH gypsum can be

facilitated under hydrothermal treatment, and speed up the crystal growth, crystallisation, and lattice perfection of calcium sulphate, promoting the release of adsorbed or incorporated iron from the solid residue and preventing it from adsorbing or incorporating again. Finally, solid-liquid separation easily extracts the liberated irons as Fe^{3+} ions (Peng, et al., 2021). Figure 2.25 shows the overall mechanism of removing iron from red gypsum.

Figure 2.25: Overall Mechanism of Removing Iron from Red Gypsum (Peng, et al., 2021).

As a result, in order to effectively extract iron from RG, both acid mineraliser and hydrothermal treatment are essential to be used. The iron metal in the RG can be removed efficiently under the optimum HTT conditions, including a liquid-solid ratio of 10, a reaction temperature of 140 °C, a reaction time of 6 hours, and 1.5 M HCl. The extraction rate of iron can achieve approximately 99% in HTT with the acid mineraliser method (Peng, et al., 2021).

2.6   Cost Analysis Method

In general, cost analysis improves project management and predicts a company's prospective earnings. Cost analysis is a method used by financial professionals to determine how much profit a project can earn compared to its entire costs. Computing a cost analysis ratio will assist a company in determining the cost and profit of a project as well as developing a financial strategy for it. The process of assessing the potential revenues from a situation or project, then removing the overall cost connected with accomplishing that situation or project, is known as cost-benefit analysis. It forecasts a project's profit and compares its cost to its expected financial advantages. Many

financial experts use cost analysis to demonstrate how much money they could make on a project (Indeed, 2021).

CHAPTER 3

METHODOLOGY AND WORK PLAN

3.1   Introduction

A literature review is critical in academic research domains because it develops and connects all prior work to provide a comprehensive perspective and appraisal and emphasise the most important discoveries. Narrative literature reviews, integrative literature reviews, and theoretical literature reviews are only a few of the many forms of literature reviews that have been developed over the years. The current study used a narrative literature review, also called a conventional literature review, representing the steps of comprehending, collecting, analysing, and evaluating prior publications on a specific topic without providing any empirical data (Green, Johnson and Adams, 2006). A literature review's main goals include identifying data that already existed in the scientific field, determining the research field's main concepts and thoughts, establishing a context for the research, determining connections between studies conducted by various researchers, and identifying gaps between publications and present situation (Pillai, 2020).

In general, a literature review is conducted for the following reasons (Boote and Beile, 2005; Karas, 2022):

    i.   Recognize the current information, perspectives, and concepts on a specific study issue.

    ii.   Determine the scope of the issue.

    iii.   Collect and correlate empirical data that is relevant to the study subject.

    iv.   Update on advances and developments in a certain study area.

    v.   Identify past study gaps and discrepancies (difficulties or flaws) that need a new investigation.

    vi.   Come up with fresh concepts, ideas, or frameworks.

3.2   Work Plan

Exploration, Interpretation, and Presentation are the three main phases of this work's methodology. The exploration stage begins with a variety of investigational procedures. After the exploration phase, the research moves on to the interpretation phase and, finally, the presentation of the findings. Figure 3.1 shows the steps involved in doing a literature review.
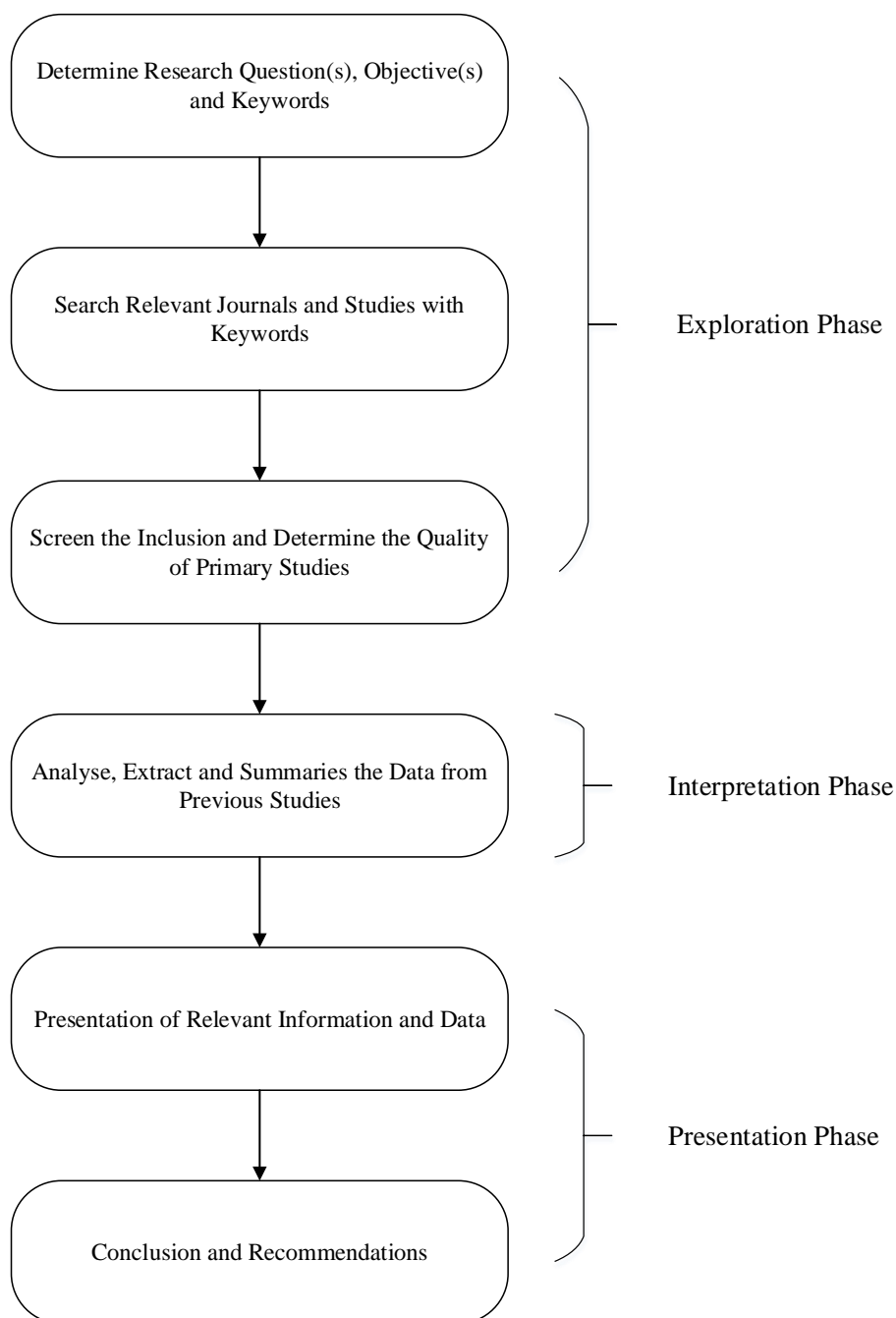
Figure 3.1: Overall Work Plan on Conducting Literature Review

3.2.1   Exploration Phase

3.2.1.1 Determining the Research Question(s), Objective(s) and Keywords

The first stage is to define why the evaluation is being conducted and what it will entail. The review's scope, interest, and value to the research field must be defined. These are the acts that have an impact on the decision of how to perform the review (Snyder, 2019). This research aims to study current work to decide the best method for red gypsum separation and perform the cost analysis of those methods to support the choice of method. As a result, a narrative literature review is more reliable and preferred than an integrative or systematic review. The review's research challenges and objectives are then developed. These are the essential points when designing the review and leading peers in a well-defined direction for the overall research so that they can avoid deviating from the topic and have a deeper understanding of the following steps, such as selecting appropriate previous findings that are relevant to the research problems (Paré and Kitsiou, 2017).

The problem statement and study objectives are determined by studying the background of plant production, the harmfulness of excessive red gypsum, and the tendency of production and economics of red gypsum. The goals of this study are to analyse the existing technologies for red gypsum separation, perform cost analysis on existing technologies and justify the best pretreatment method for red gypsum separation.

3.2.1.2 Search Relevant Journals and Studies with Keywords

Search strategy should be established before searching the appropriate journals, such as search phrases, publication dates, sources, and inclusion and exclusion criteria. These choices are critical and will reflect the review's quality (Snyder, 2019). In general, journal publication dates will be better in these five years in order to ensure that the material and data collected remain current. However, reducing the publishing date may result in missing components in developing the study topic. As a result, the search technique may change based on the information available.

This review utilises a variety of web sources to gather important information on the issue of pretreatment of red gypsum. The relevant research

is available by searching the terms "red gypsum", "extracting iron from red gypsum", "acid leaching", "hydrothermal treatment", "mineral carbonation" and "application of red gypsum" with the date of publication that is within ten years. Furthermore, the data and information reported in this study are taken from freely available e-books and online journal websites. UTAR e-databases provides access to the majority of the following online resources:

   i.   ACS Publication (https://pubs-acs-org.libezp2.utar.edu.my/)
   ii.   Elsevier (https://www.elsevier.com/open-access/open-access-journals)
   iii. ResearchGate (https://www.researchgate.net/)
   iv.   Science Direct (https://www-sciencedirect-com.libezp2.utar.edu.my/)
   v.   Scopus (https://www-scopus-com.libezp2.utar.edu.my/)
   vi.   Semantic Scholar (https://www.semanticscholar.org/)
   vii. Springer link (https://link-springer-com.libezp2.utar.edu.my/)
   viii. UTAR E-journals Website (https://library.utar.edu.my/)
   ix.   Wiley Online Library (https://onlinelibrary-wiley-com.libezp2.utar.edu.my/)

3.2.1.3 Screen the Inclusion and Determine the Quality of Primary Studies

Moreover, the quality of studies published is crucial for performing a literature review since high-quality primary studies provide detailed information of interest and provide thoughts and insights that go far beyond previous studies' recital. A large number of relevant journals were gathered in the previous stage by using the searching approach strategies. Then, based on the criteria for inclusion and exclusion, each journal's applicability and relevancy are determined to guarantee the relationship between collected data and research objectives, hence reducing digressions and errors (Brocke, et al., 2009). Furthermore, the obtained data is managed with Mendeley Software, designed for more accessible citations and references and provides the most recent and connected publications through sources for related materials. Figure 3.2 shows the Mendeley Software.
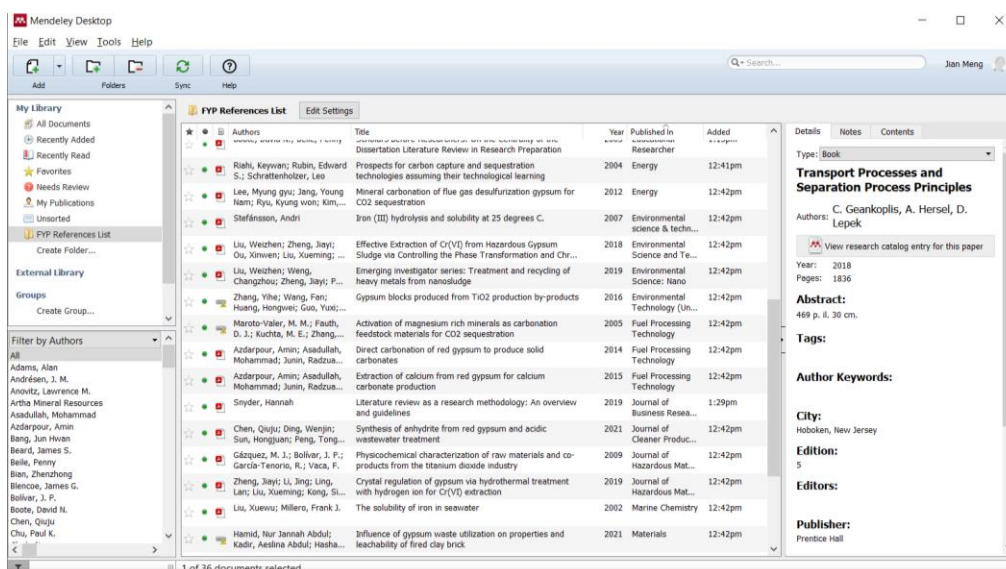
Figure 3.2: Mendeley Software

3.2.2 Interpretation Phase

The interpretation is carried out at this level through the analytical and abstract processes. This implies that the selected information and data retrieved in the preceding phases are analysed and merged into a cohesive narrative based on the review's objectives, such as notable results and empirical study correlations or connections. The data gathered and produced must be straightforward and understandable to comprehend for others. The data must be organised in such a way that it may be used to draw attention to existing research. The overall trend of the research can be determined, but contradictions between them must be noted (Cronin, 2011; Templier and Paré, 2015).

3.2.3 Presentation of Relevant Information and Data

Depending on the type of material and information and the level of sophistication, presenting a review can be done in a variety of ways. By acquiring and synthesising relevant documents, it can produce a complete summary of the issue of interest. Numerous standards describe how to perform a quantitative or qualitative literature review. The current work uses a qualitative approach to focus on the separation techniques and the characterisation of red gypsum while using a quantitative approach to focus on the cost analysis for existing techniques and the extraction rate of iron from the red gypsum (Paré and Kitsiou, 2017).

3.3 Journals Reviewed in this Study

A total of 80 articles or journals are reviewed in this study. As mentioned in **Section 3.2.1.2**, the ideal journals/articles publication date reviewed are within ten years (from the year 2013 to the year 2022). There are 48 articles/journals with a publication date from the year 2013 to the year 2022 are reviewed. However, some results or data will be missed if no researchers did the related study within the ten years. Therefore, although some articles/journals have an earlier publication date, they are reliable and will be reviewed in this study. A total of 32 numbers of articles/journals are reviewed from the year 1989 to the year 2012. Among the 32 articles/journals, there are only three reviewed journals published in the 20th century (from the year 1989 to the year 2000). Figure 3.3 shows the number of reviewed articles/journals by each year.
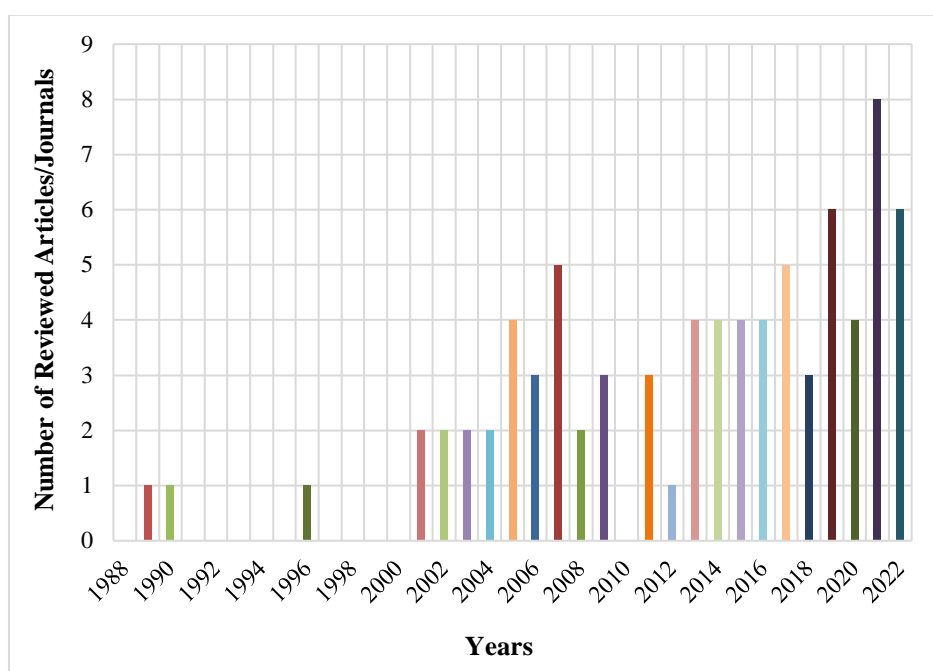
Figure 3.3:   Number of Reviewed Articles/Journals by Years.

CHAPTER 4

RESULTS AND DISCUSSION

4.1   Cost Analysis

As mentioned in **Section 2.6**, the cost analysis demonstrates to clients how much money they could make on a project. Therefore, the cost analysis was performed in this study to justify the cost-effectiveness of each treatment method. In this study, only material and energy costs were performed in the following section. As the cost has to be compared between three treatment methods, several assumptions were made as follows:

    i.   10 g of red gypsum were used for calculation, then the final cost was converted into one tonne of red gypsum basis.

    ii.   The composition of red gypsum was standardised to follow Table 2.1.

    iii.   The ambient temperature of Malaysia was assumed to be 30 °C.

    iv.   In the material preparation stage, prior to the autoclave reactor, the red gypsum was heated to 45 °C so that the red gypsum was entirely dry, homogenised and ground. Therefore, the initial temperature of red gypsum was assumed to be 45 °C.

    v.   Heating duty was equivalent to electricity duty.

    vi.   The price of electricity in Malaysia was retrieved from Global Petrol Prices (2021), which is RM 0.388 per kWh.

4.1.1   Total Cost of Mineral Carbonation Method

4.1.1.1 Material Cost of Mineral Carbonation Method

The only material used in the mineral carbonation of red gypsum was carbon dioxide. The amount of CO_2 could be estimated based on the two chemical equations (2.5 and 2.6) shown in **Section 2.3.3**.

$$Fe(OH)_2 + CO_2 \rightarrow FeCO_3 + H_2O \qquad (2.5)$$
$$CaSO_4 + CO_2 + H_2O \rightarrow H_2SO_4 + CaCO_3 \qquad (2.6)$$
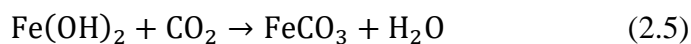
Based on Table 2.1, the composition of Fe^{2+} and Ca^{2+} was estimated to be 16.04% and 26.36%, respectively. As 10 g of red gypsum was used, so 1.604 g of Fe^{2+} and 2.636 g of Ca^{2+} were reacted. The molar mass and the number of moles was estimated and tabulated in Table 4.1.

Table 4.1: Number of Mole of Fe^{2+} and Ca^{2+}.

	Fe^{2+}	Ca^{2+}
Mass (g)	1.604	2.636
Molar Mass (g/mol)	55.845	40.078
Mole (mole)	0.02872	0.06577

Since both Fe^{2+} and Ca^{2+} used one mole, respectively to react with one mole of CO_2, the total number of moles of CO_2 required is 0.09449 mol. Since the molar mass of carbon dioxide was 44.01 g/mol, the required CO_2 mass to react with 10 g of red gypsum was 4.158 g. When scaled up to 1 tonne of red gypsum, the mass of CO_2 required becomes 0.4158 tonnes. According to Pharmacompass (2022a), the price of CO_2 could be estimated as RM 30.61 per kg. Therefore, the material cost of mineral carbonation treatment for one tonne of red gypsum was RM 12727.64.

4.1.1.2 Energy Cost of Mineral Carbonation Method

Generally, carbon dioxide (CO_2) is in the liquid phase when stored, transported and handled. It is either at room temperature with a pressure of 45 bar to 65 bar or refrigerated with a temperature of –35 °C to –15 °C and pressures of 12 bar to 25 bar (Linde, 2017). Assuming that the carbon dioxide used was in the temperature of 25 °C and the pressure of 65 bar. The energy involved in the calculation is as follows:

      i.   Increasing the pressure of CO_2 to 70 bar.

      ii.   Heating the reactants ($Fe(OH)_2$, $CaSO_4$ and CO_2) to 200 °C.

      iii.   Maintaining the reaction temperature at 200 °C.

      iv.   Cooling down the product to the ambient temperature of 30 °C.

Increasing the pressure of CO_2 to 70 bar.

Firstly, the energy needed to increase the CO_2 pressure was calculated by using Heuristic 39 (Seider, et al., 2017). Equation 4.1 showed the estimation of power in horsepower (Hp) for pumping a liquid.

$$P = \frac{F(\Delta P)}{1714} \qquad (4.1)$$

where,

P = power, Hp

F = flowrate, gpm

ΔP = differential pressure, psi

The flowrate of CO_2 (gpm) could be calculated using the mass of CO_2 divided by the reaction time of 60 minutes and its density of 780.5 kg/m^3.

$$\text{Flowrate of } CO_2, F = \frac{4.158 \text{ g}}{60 \text{ minutes}} \times \frac{\text{m}^3}{780.5 \text{ kg}} \times \frac{\text{kg}}{1000 \text{ g}} \times \frac{264.2 \text{ gallons}}{\text{m}^3}$$
$$= 2.346 \times 10^{-5} \text{ gpm}$$

The differential pressure in bar was 5, which was equivalent to 72.52 psi. Therefore, the estimation power used for increasing pressure of CO_2 to 70 bar could be estimated as follow:

$$P = \frac{(2.346 \times 10^{-5} \text{ gpm})(72.52 \text{ psi})}{1714}$$
$$= 9.926 \times 10^{-7} \text{Hp (or } 7.402 \times 10^{-7} \text{ kW)}$$

Heating the reactants ($Fe(OH)_2$, $CaSO_4$ and CO_2) to 200 °C.

Secondly, the reactants were needed to be heated up to the operating temperature of 200 °C. The initial temperature of CO_2 was 25 °C and it was in the liquid state. The heat capacity of liquid CO_2 could be estimated by using Kopp's rule, a simple empirical approach for determining a solid's or liquid's heat capacity at around 20 °C (Felder, Rousseau and Bullard, 2016). Atomic

heat capacity data for Kopp's rule was tabulated in Table 4.2. The heat capacity of liquid CO_2 could be calculated by using Equation 4.2.

$$\left(C_p\right)_{CO_2,l} = \left(C_{pa}\right)_C + 2\left(C_{pa}\right)_O \tag{4.2}$$

where,

$\left(C_p\right)_{CO_2}$ = Heat capacity of liquid CO_2, J/(mol·°C)

$\left(C_{pa}\right)_C$ = Atomic heat capacity of C, J/(g·atom·°C)

$\left(C_{pa}\right)_O$ = Atomic heat capacity of O, J/(g·atom·°C)

Table 4.2: Atomic heat capacity data for Kopp's rule (Felder, Rousseau and Bullard, 2016).

Elements	$C_{pa}[\text{J}/(\text{g} \cdot \text{atom} \cdot °\text{C})]$
C	12
O	25

$$\left(C_p\right)_{CO_2,l} = \left(C_{pa}\right)_C + 2\left(C_{pa}\right)_O$$

$$\left(C_p\right)_{CO_2,l} = 12 + 2(25) = 62 \text{ J}/(\text{mol} \cdot °\text{C})$$

Since the boiling point of CO_2 at 70 bar was 28.66 °C, so the heat required to increase liquid °C from 25 °C to 28.66 °C could be estimated by using Equation 4.3.

$$\Delta H = N_{CO_2} \int_{25\,°C}^{28.66\,°C} \left(C_p\right)_{CO_2,l} dT \tag{4.3}$$

$$\Delta H = 0.09449 \times \int_{25}^{28.66} 62 \, dT = 0.09449 \times 62 \times (28.66 - 25)$$

$$\Delta H = 21.44 \text{ J}$$

where,

ΔH = Heat required, J

N_{CO_2} = Number of moles of carbon dioxide, mol

$\left(C_p\right)_{CO_2,l}$ = Heat capacity of liquid CO_2, J/(mol·°C)

According to NIST (2017), the heat of vaporisation of CO_2 was assumed to be 16.7 kJ/mol. So, the heat required to change its liquid phase into gas phase was around 1.578 kJ. The carbon dioxide was now in the gas phase with a temperature of 28.66 °C and a pressure of 70 bar. The initial temperature of $Fe(OH)_2$ and $CaSO_4$ were 45 °C. The heat capacity data of $Fe(OH)_2$, $CaSO_4$ and gas phase CO_2, as well as sample calculation of sensible heat were performed in Appendix A. Table 4.3 showed the heat duty of heating up the reactants ($Fe(OH)_2$, $CaSO_4$ and CO_2) to 200 °C.

Table 4.3: Heat Duty of Heating the Reactants ($Fe(OH)_2$, $CaSO_4$ and CO_2) to 200 °C.

Reactants		Heat Capacity (J/mol · K)	Mole (mole)	Heat Duty (kJ)
	$Fe(OH)_2$	13950	0.02872	0.4006
	$CaSO_4$	16972	0.06577	1.116
CO_2	Liquid phase	-		0.02144
	Vaporisation	-		1.578
	Gas phase	8350	0.09449	0.7890
	TOTAL			3.905

Maintaining the reaction temperature at 200 °C.

Thirdly, the reaction temperature was needed to maintain at 200 °C. The algorithm of energy balance was described based on a hypothetical pathway, as shown in Figure 4.1.
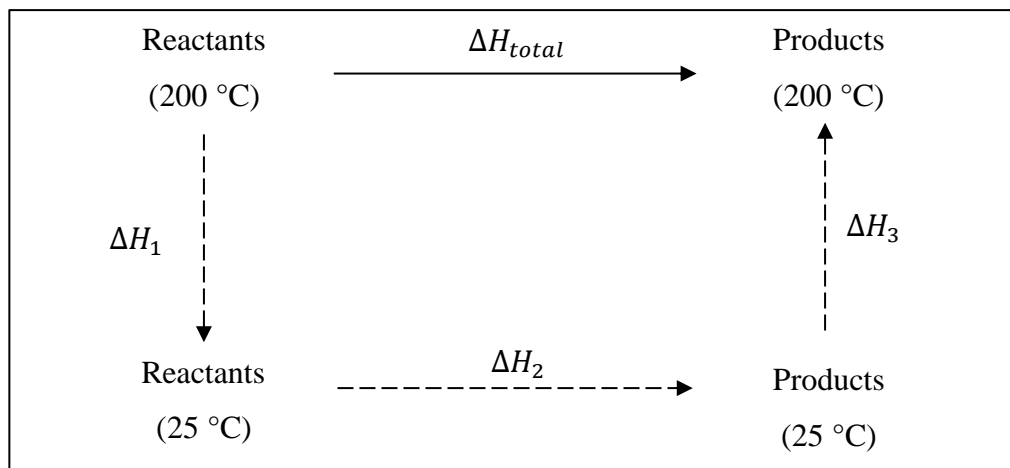
Figure 4.1: Hypothetical Process Pathway of Mineral Carbonation.

There was a total of three reactants have to cool down from 200 °C to 25 °C, which included $Fe(OH)_2$, $CaSO_4$, CO_2 and H_2O according to Equations 2.5 and 2.6. The calculation of heat released of $Fe(OH)_2$, $CaSO_4$, CO_2 and H_2O could refer to the sample calculation of sensible heat performed in Appendix A. Table 4.4 showed the ΔH_1 of reactants ($Fe(OH)_2$, $CaSO_4$, CO_2 and H_2O).

Table 4.4: ΔH_1 of reactants ($Fe(OH)_2$, $CaSO_4$, CO_2 and H_2O).

Reactants	Heat Capacity (J/mol · K)	Mole (mole)	Heat Duty (kJ)
$Fe(OH)_2$	−15750	0.02872	−0.4523
$CaSO_4$	−18950	0.06577	−1.246
H_2O	−5862	0.06577	−0.3855
CO_2	−8526	0.09449	−0.8056
	TOTAL		−2.889

The heat of reaction of this process was based on Equations 2.5 and 2.6. The data for standard heat of formation for each component involved were tabulated in Table 4.5.

Table 4.5: Heat of Formation of Chemicals Involved (Lemire et al., 2013; Koretsky, 2013; Felder, Rousseau and Bullard, 2016).

Components	Heat of Formation (kJ/mol)	Sources
$FeCO_3$	−752.61	(Lemire, et al., 2013)
$Fe(OH)_2$	−583.39	
$CaSO_4$	−1434.11	(Koretsky, 2013)
CO_2	−393.51	
H_2O	−285.83	
H_2SO_4	−813.99	
$CaCO_3$	−1206.9	(Felder, Rousseau and Bullard, 2016)

The extraction rate of iron and calcium were 26.31% and 41.04%, so the heat of reactions for Equations 2.5 and 2.6 were calculated as follows:

$$\Delta H_{2,R2.5} = \xi_{2.5}\left[\left(\Delta h_{f,298}^\circ\right)_{H_2O} + \left(\Delta h_{f,298}^\circ\right)_{FeCO_3} - \left(\Delta h_{f,298}^\circ\right)_{CO_2}\right.$$
$$\left. - \left(\Delta h_{f,298}^\circ\right)_{Fe(OH)_2}\right]$$
$$\Delta H_{2,R2.5} = 0.2631(-285.83 - 752.61 + 393.51 + 583.39) = -16.19 \text{ kJ}$$

$$\Delta H_{2,R2.6} = \xi_{2.6}\left[\left(\Delta h_{f,298}^\circ\right)_{CaCO_3} + \left(\Delta h_{f,298}^\circ\right)_{H_2SO_4} - \left(\Delta h_{f,298}^\circ\right)_{H_2O}\right.$$
$$\left. - \left(\Delta h_{f,298}^\circ\right)_{CO_2} - \left(\Delta h_{f,298}^\circ\right)_{CaSO_4}\right]$$
$$\Delta H_{2,R2.6} = 0.4104(-1206.9 - 813.99 + 285.83 + 393.51 + 1434.11)$$
$$\Delta H_{2,R2.6} = 37.99 \text{ kJ}$$

$$\Delta H_2 = \Delta H_{2,R2.5} + \Delta H_{2,R2.6} = -16.19 + 37.99 = 21.80 \text{ kJ}$$

There was a total of seven products and unreacted reactants have to heat up from 25 °C to 200 °C, which included $Fe(OH)_2$, $CaSO_4$, CO_2, H_2O, $FeCO_3$, $CaCO_3$ and H_2SO_4. The calculation of heat absorbed could refer to the sample calculation of sensible heat performed in Appendix A. Table 4.6 showed the ΔH_3 of unreacted reactants and products.

Table 4.6: ΔH_3 of unreacted reactants and products ($Fe(OH)_2$, $CaSO_4$, CO_2, H_2O, $FeCO_3$, $CaCO_3$ and H_2SO_4).

Reactants	Heat Capacity (J/mol · K)	Mole (mole)	Heat Duty (kJ)
$Fe(OH)_2$	15750	0.02117	0.3334
$CaSO_4$	18950	0.03878	0.7349
H_2O	5862	0.04634	0.2716
CO_2	8526	0.05995	0.5111
$FeCO_3$	16286	0.00756	0.1231
$CaCO_3$	19528	0.02699	0.5271
H_2SO_4	25395	0.02699	0.6854
	TOTAL		3.187

$$\Delta H_{total} = \Delta H_1 + \Delta H_2 + \Delta H_3 = -2.889 + 21.80 + 3.187 = 22.10 \text{ kJ}$$

The heat duty needed to maintain the reaction temperature at 200 °C was 22.10 kJ.

Cooling down the product to the ambient temperature of 30 °C

Lastly, the products were needed to be cooled down to the ambient temperature of 30 °C. The calculation of heat duty of $Fe(OH)_2$, $CaSO_4$, CO_2, H_2O, $FeCO_3$, $CaCO_3$ and H_2SO_4 could refer to the sample calculation of sensible heat performed in Appendix A. Table 4.7 showed the heat duty of cooling down the products ($Fe(OH)_2$, $CaSO_4$, CO_2, H_2O, $FeCO_3$, $CaCO_3$ and H_2SO_4) to 30 °C.

Table 4.7: Heat Duty of Cooling Down the Products ($Fe(OH)_2$, $CaSO_4$, CO_2, H_2O, $FeCO_3$, $CaCO_3$ and H_2SO_4) into 30 °C.

Reactants	Heat Capacity (J/mol · K)	Mole (mole)	Heat Duty (kJ)
$Fe(OH)_2$	−15300	0.02117	−0.3239
$CaSO_4$	−18461	0.03878	−0.7159
H_2O	−5700	0.04634	−0.2641
CO_2	−8286	0.05995	−0.4967
$FeCO_3$	−15872	0.00756	−0.1200
$CaCO_3$	−15755	0.02699	−0.4252
H_2SO_4	−24676	0.02699	−0.6660
TOTAL			−3.012

The conversion factor of kJ to kWh was 1/3600. Table 4.8 showed the total kilowatt-hour required for mineral carbonation of red gypsum. From Table 4.8, it was clearly stated that treating 10 g of red gypsum by using the mineral carbonation method required 8.061×10^{-3} kWh. When scaling up into treating one tonne of red gypsum, 806.1 kWh was required. Since the price of electricity in Malaysia was retrieved from Global Petrol Prices (2021) which was RM 0.388 per kWh. Therefore, the energy cost of mineral carbonation treatment for one tonne of red gypsum was RM 312.77.

Table 4.8: Total Kilowatt-hour Required in Mineral Carbonation of Red Gypsum.

	Heat Duty (kJ)	Power (kWh)
Increasing the pressure of CO_2 to 70 bar.	-	7.402×10^{-7}
Heating the reactants to 200 °C.	3.905	1.085×10^{-3}
Maintaining the reaction temperature at 200 °C.	22.10	6.139×10^{-3}
Cooling down the product to the ambient temperature.	3.012	8.367×10^{-4}
TOTAL		8.061×10^{-3}

4.1.2 Total Cost of Acid Leaching Method

The parameters used in the estimation of cost for the acid leaching method were a solid-liquid ratio of 1:12.5, a reaction temperature of 70 °C, a reaction time of 60 minutes, and a 0.5 M H_2SO_4 concentration in order to achieve a 93.14% of extraction rate according to Jiang, Sun and Peng (2019).

4.1.2.1 Material Cost of Acid Leaching Method

The materials used in the acid leaching method were water and sulphuric acid. The amount of water and H_2SO_4 could be estimated based on the solid-liquid ratio of 1:12.5. 10 g of red gypsum was required 125 ml of 0.5 M H_2SO_4 and water. The purchased H_2SO_4 has 98% (w/w), equivalent to 18.4 molarity (Nest Group, 2021). The purchased H_2SO_4 was then needed to mix with water to produce 0.5 M H_2SO_4. The volume used for purchased H_2SO_4 when 10 g of red gypsum was treated, could be calculated by Equation 4.4.

$$M_1 V_1 = M_2 V_2 \qquad (4.4)$$

where,

M_1 = Molarity of Purchased Acid, M

M_2 = Molarity of Dilute Acid, M

V_1 = Volume of Purchased Acid, ml

V_2 = Volume of Dilute Acid, ml

$$M_1 V_1 = M_2 V_2$$
$$(18.4 \text{ M}) \times V_1 = (0.5 \text{ M}) \times (125 \text{ ml})$$
$$V_1 = 3.397 \text{ ml}$$

From the calculation, 10 g of red gypsum was required 3.397 ml of purchased H_2SO_4 with 121.6 ml of water. Since the density of H_2SO_4 and water was 1.83 g/ml and 1.0 g/ml, so the mass of purchase H_2SO_4 and water needed was 6.216 g and 121.6 g, respectively. When scaled up to 1 tonne of red gypsum, the mass of H_2SO_4 and water required becomes 0.6216 tonne and 12.16 tonnes, respectively. According to Pharmacompass (2022c), the price of

H_2SO_4 could be estimated as RM 7.15 per kg. Therefore, the cost of 0.6216 tonne H_2SO_4 was RM 4444.44. Besides, according to Bernama (2020), one thousand litres of water had a value of RM 1.38. The volume of 12.16 tonnes of water was equivalent to 12160 litres, so the cost of water was RM 16.78. Thus, the material cost of the acid leaching method for one tonne of red gypsum was RM 4461.22.

4.1.2.2 Energy Cost of Acid Leaching Method

The energy used could be estimated based on the chemical equation 2.7, as shown in **Section 2.4.2**.

$$2Fe(OH)_3 + 3H_2SO_4 \longrightarrow Fe_2(SO_4)_3 + 6H_2O \qquad (2.7)$$
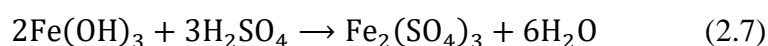
Before energy cost calculation, the number of moles of Fe^{3+} was obtained from Table 4.1 which was 0.02872 mol. Since 2 moles of $Fe(OH)_3$ reacted with 3 moles of H_2SO_4, so the total number of moles of H_2SO_4 required was 0.04308 mol. The energy involved in the calculation was as follows:

    i.   Heating the reactants $Fe(OH)_3$ and H_2SO_4 from 45 °C and 30 °C, respectively to 70 °C.

    ii.   Maintaining the reaction temperature at 70 °C.

    iii.   Cooling down the product to the ambient temperature of 30 °C.

Heating the reactants Fe(OH)₃ and H₂SO₄ from 45 •C and 30 •C, respectively to 70 •C.

Firstly, the reactants were needed to be heated up to the operating temperature of 200 °C. The calculation of heat duty of $Fe(OH)_3$ and H_2SO_4 could refer to the sample calculation of sensible heat that was performed in Appendix A. Table 4.9 showed the heat duty of heating the reactants ($Fe(OH)_3$ and H_2SO_4) to 70 °C.

Table 4.9: Heat Duty of Heating the Reactants ($Fe(OH)_3$ and H_2SO_4) into 70 °C.

Reactants	Heat Capacity (J/mol · K)	Mole (mole)	Heat Duty (kJ)
$Fe(OH)_3$	3800	0.02872	0.1091
H_2SO_4	5766	0.04308	0.2484
	TOTAL		0.3575

Maintaining the reaction temperature at 70 °C.

Secondly, the reaction temperature was needed to maintain at 70 °C. The algorithm of energy balance was described based on a hypothetical pathway, as shown in Figure 4.2.
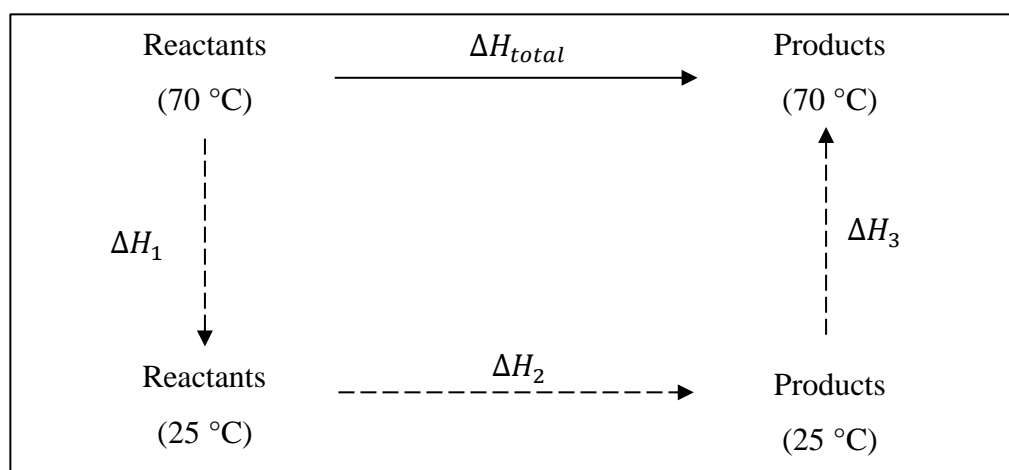
Figure 4.2: Hypothetical Process Pathway of Acid Leaching.

There was a total of two reactants have to cool down from 70 °C to 25 °C, which included $Fe(OH)_3$ and H_2SO_4 according to Equation 2.7. The calculation of heat released of $Fe(OH)_3$ and H_2SO_4 could refer to the sample calculation of sensible heat that was performed in Appendix A. Table 4.10 showed the ΔH_1 of reactants ($Fe(OH)_3$ and H_2SO_4).

Table 4.10: ΔH_1 of reactants (Fe(OH)$_3$ and H$_2$SO$_4$).

Reactants	Heat Capacity (J/mol · K)	Mole (mole)	Heat Duty (kJ)
Fe(OH)$_3$	−6840	0.02872	−0.1964
H$_2$SO$_4$	−6485	0.04308	−0.2794
	TOTAL		−0.4758

The heat of reaction of this process was based on Equation 2.7. The data for standard heat of formation for each component involved were tabulated in Table 4.11.

Table 4.11: Heat of Formation of Chemicals Involved (Lemire, et al., 2013; Koretsky, 2013).

Components	Heat of Formation (kJ/mol)	Sources
Fe(OH)$_3$	−829.9	(Lemire, et al., 2013)
Fe$_2$(SO$_4$)$_3$	−2584.1	
H$_2$SO$_4$	−813.99	(Koretsky, 2013)
H$_2$O	−285.83	

The extraction rate of iron is 93.14%, so the heat of reaction for Equation 2.7 was calculated as follows.

$$\Delta H_{2,R2.7} = \xi_{2.7} \left[3\left(\Delta h_{f,298}^{\circ}\right)_{\text{H}_2\text{O}} + 0.5\left(\Delta h_{f,298}^{\circ}\right)_{\text{Fe}_2(\text{SO}_4)_3} - 1.5\left(\Delta h_{f,298}^{\circ}\right)_{\text{H}_2\text{SO}_4} \right.$$
$$\left. - \left(\Delta h_{f,298}^{\circ}\right)_{\text{Fe(OH)}_3} \right]$$
$$\Delta H_{2,R2.7} = 0.9314[3 \times (-285.83) + 0.5 \times (-2584.1) - 1.5 \times (-813.99)$$
$$- (-829.9)] = -91.89 \text{ kJ}$$

There were four products and unreacted reactants have to heat up from 25 °C to 70 °C, which included Fe(OH)$_3$, H$_2$SO$_4$, Fe$_2$(SO$_4$)$_3$ and H$_2$O. The calculation of heat absorbed could refer to the sample calculation of sensible heat that was performed in Appendix A. Table 4.12 showed the ΔH_3 of unreacted reactants and products.

Table 4.12: ΔH_3 of unreacted reactants and products ($Fe(OH)_3$, H_2SO_4, $Fe_2(SO_4)_3$ and H_2O).

Reactants	Heat Capacity (J/mol · K)	Mole (mole)	Heat Duty (kJ)
$Fe(OH)_3$	6840	0.00197	0.01347
$Fe_2(SO_4)_3$	12788	0.01338	0.1711
H_2SO_4	6485	0.00296	0.01920
H_2O	1472	0.08026	0.1181
	TOTAL		0.3219

$$\Delta H_{total} = \Delta H_1 + \Delta H_2 + \Delta H_3 = -0.4758 - 91.89 + 0.3219 = -92.04 \text{ kJ}$$

The heat duty needed to maintain the reaction temperature at 70 °C was –92.04 kJ.

Cooling down the product to the ambient temperature of 30 °C

Lastly, the products were needed to be cooled down to the ambient temperature of 30 °C. The calculation of heat duty of $Fe(OH)_3$, H_2SO_4, $Fe_2(SO_4)_3$ and H_2O could refer to the sample calculation of sensible heat that was performed in Appendix A. Table 4.13 showed the heat duty of cooling down the products ($Fe(OH)_3$, H_2SO_4, $Fe_2(SO_4)_3$ and H_2O) to 30 °C.

Table 4.13: Heat Duty of Cooling Down the Products ($Fe(OH)_3$, H_2SO_4, $Fe_2(SO_4)_3$ and H_2O) into 30 °C.

Reactants	Heat Capacity (J/mol · K)	Mole (mole)	Heat Duty (kJ)
$Fe(OH)_3$	–6080	0.00197	–0.01198
$Fe_2(SO_4)_3$	–11417	0.01338	–0.1528
H_2SO_4	–5766	0.00296	–0.01707
H_2O	–1310	0.08026	–0.1051
	TOTAL		–0.2870

The conversion factor of kJ to kWh was 1/3600. Table 4.14 showed the total kilowatt-hour required for the acid leaching method. From Table 4.14, it was clearly stated that treating 10 g of red gypsum by using the acid

leaching method required 2.575×10^{-2} kWh. When scaling up into treating one tonne of red gypsum, 2575 kWh was required. Since the price of electricity in Malaysia was retrieved from Global Petrol Prices (2021) which was RM 0.388 per kWh. Therefore, the energy cost of the acid leaching method for one tonne of red gypsum was RM 999.10.

Table 4.14: Total Kilowatt-hour Required in Acid Leaching Method.

	Heat Duty (kJ)	Power (kWh)
Heating the reactants to 70 °C.	0.3575	9.931×10^{-5}
Maintaining the reaction temperature at 70 °C.	92.04	2.557×10^{-2}
Cooling down the product to the ambient temperature.	0.2870	7.972×10^{-5}
TOTAL		2.575×10^{-2}

4.1.3   Total Cost of Hydrothermal Treatment Method

The parameters used in the estimation of cost for the hydrothermal treatment method were a liquid-solid ratio of 10, a reaction temperature of 140 °C, a reaction time of 6 hours, and 1.5 M HCl concentration in order to achieve approximately 99% of the extraction rate according to Peng, et al. (2021).

4.1.3.1   Material Cost of Hydrothermal Treatment Method

The materials used in the hydrothermal treatment method were water and hydrochloric acid. The amount of water and HCl could be estimated based on the liquid-solid ratio of 10. 10 g of red gypsum was required 100 ml of 1.5 M HCl and water. The purchased HCl has only 36% (w/w), equivalent to 11.65 molarity (Nest Group, 2021). The purchased HCl was then needed to mix with water to produce 1.5 M HCl. The volume used for purchased HCl when 10 g of red gypsum was treated, could be calculated by Equation 4.4.

$$M_1 V_1 = M_2 V_2$$
$$(11.65 \text{ M}) \times V_1 = (1.5 \text{ M}) \times (100 \text{ ml})$$
$$V_1 = 12.87 \text{ ml}$$

From the calculation, 10 g of red gypsum was required 12.87 ml of purchased HCl with 87.13 ml of water. Since the density of HCl and water was 1.18 g/ml and 1.0 g/ml, so the mass of purchased HCl and water needed was 15.19 g and 87.13 g, respectively. When scaled up to 1 tonne of red gypsum, the mass of HCl and water required becomes 1.519 and 8.713 tonnes, respectively. The amount of HCl and water calculated in this section was consistent with Peng, et al. (2021). According to Pharmacompass (2022b), the price of HCl could be estimated as RM 4.20 per kg. Therefore, the cost of 1.519 tonne HCl was RM 6379.80. Besides, according to Bernama (2020), one thousand litres of water had a value of RM 1.38. The volume of 8.713 tonnes of water was equivalent to 8713 litres, so the cost of water was RM 12.02. Thus, the material cost of the hydrothermal treatment method for one tonne of red gypsum was RM 6391.82.

4.1.3.2   Energy Cost of Hydrothermal Treatment Method

As hydrothermal treatment in this study was a technique to dissolve iron impurities into the water with mineraliser, it would not have the chemical equation. Hence, the energy cost of hydrothermal treatment would be mainly based on the heat of dissolution of iron impurities into the water with mineraliser. However, since no experiment was conducted in this study and no data on the heat of dissolution of iron impurities into the water with hydrochloric acid, the energy cost was assumed to be the same as the energy cost performed by Peng, et al. (2021). They stated the energy cost for this method based on 1 tonne of red gypsum was around 105.6 CNY which is equivalent to RM 70.03.

4.1.4   Summary of Total Cost from Various Methods

Table 4.15 showed the total cost of mineral carbonation, acid leaching and hydrothermal treatment methods.

Table 4.15: Summary of Total Cost.

	Mineral Carbonation	Acid Leaching	Hydrothermal Treatment
Material Cost (RM)	12727.64	4461.22	6391.82
Energy Cost (RM)	312.77	999.10	70.03
Total Cost (RM)	13040.41	5460.32	6461.85

4.2 Justification of the Best Pretreatment of Red Gypsum

Mineral carbonation, acid leaching, and hydrothermal treatment were compared based on environmental, efficiency and cost aspects to justify the best pretreatment of RG.

4.2.1 Environmental Aspect

The mineral carbonation method had no negative impact on the environment among these three treatment methods. The primary objective of mineral carbonation was to store the carbon dioxide in the form of stable solid carbonates, so the global GHG was lowered. Besides, the form of mineral carbonates was not temporary storage since the products of mineral carbonation were thermodynamically stable. Therefore, two environmental issues could be solved at once: reducing the GHG (CO_2) and reutilising industrial wastes (RG).

In the acid leaching of red gypsum, sulphuric acid (a strong acid) was used as one of the reactants. Therefore, the products of the acid leaching method included natural gypsum and acidic filtrate, which consisted of $Fe_2(SO_4)_3$ and unreacted sulphuric acid. Although the acidic filtrate could be neutralised by adding calcium oxide (CaO) or calcium hydroxide ($Ca(OH)_2$) by adjusting the pH value in the range of 3.5 to 4.5 and precipitating the $Fe(OH)_3$, it was still considered a weaker acidic filtrate. Thus, the acid leaching method had the potential for secondary pollution. Similarly, hydrochloric acid was a strong acid and was used as one of the materials in the hydrothermal treatment method. The products of this technology included natural gypsum and concentrated iron liquid, as shown in Figure 2.25. The concentrated iron liquid consisted of not only iron but also hydrochloric acid.

Therefore, the hydrothermal treatment method had the potential for secondary pollution as well.

The hydrothermal treatment method had a more negative impact on the environment than the acid leaching method. The sulphuric acid had a lower pKa value which was –3 than the hydrochloric acid's pKa value of –6.3, indicating that the strength of hydrochloric acid was stronger than that of sulphuric acid. Although sulphuric acid was a diprotic acid that released two protons per one sulphuric acid molecule, only the dissociation of the first proton indicated that it was a strong acid. After dissociation of the first proton, HSO_4^- was produced and it was considered a weak acid with a pKa value of 1.92. The ionisations of sulphuric acid and hydrochloric acid were shown in Equations 4.5, 4.6 and 4.7 (Lumen, 2022; Zumdahl, 2003; Madhusha, 2017).

$$H_2SO_4 + H_2O \rightarrow HSO_4^- + H_3O^+ \tag{4.5}$$

$$HSO_4^- + H_2O \rightarrow SO_4^{2-} + H_3O^+ \tag{4.6}$$

$$HCl + H_2O \rightarrow Cl^- + H_3O^+ \tag{4.7}$$
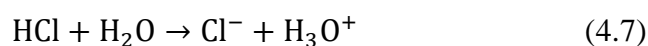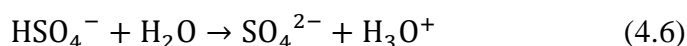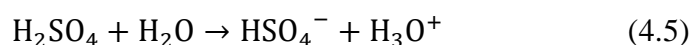
Furthermore, the concentration of sulphuric acid used in the acid leaching method was 0.5 M, while the concentration of hydrochloric acid used in hydrothermal treatment was 1.5 M. According to Mountholyoke (2005), acid strength and its concentration were the critical parameters used to determine the corrosivity of acid. Therefore, hydrochloric acid had higher corrosivity than sulphuric acid as both strength and concentration of hydrochloric acid were higher. In a nutshell, the mineral carbonation method had no impact on the environment, followed by acid leaching and hydrothermal treatment methods.

4.2.2   Efficiency Aspect

Among these three pretreatment methods, mineral carbonation had the lowest extraction rate of iron, followed by acid leaching and hydrothermal treatment method. The extraction rate of mineral carbonation, acid leaching and hydrothermal treatment methods was 26.31%, 93.14% and 99%, respectively. As mentioned in **Section 2.2.4**, three different shapes, which included strips, plate-shaped particles, and irregular blocks, could be seen in the SEM image

of the red gypsum (Figure 2.3 and Figure 2.4). The long or plate-shaped particles in the SEM image indicated gypsum crystals, while the irregular fine particles or agglomerates indicated the presence of iron and other impurities.

The SEM image could support the result of efficiency in acid leaching and hydrothermal treatment. Since the extraction rate of mineral carbonation was very low, no researchers performed its characterisation of the products. It could be observed from Figure 4.3, that most of the agglomerates were removed compared to Figure 2.3. However, the products after acid leaching still consisted of some agglomerates, indicating that some iron and other impurities were not removed.
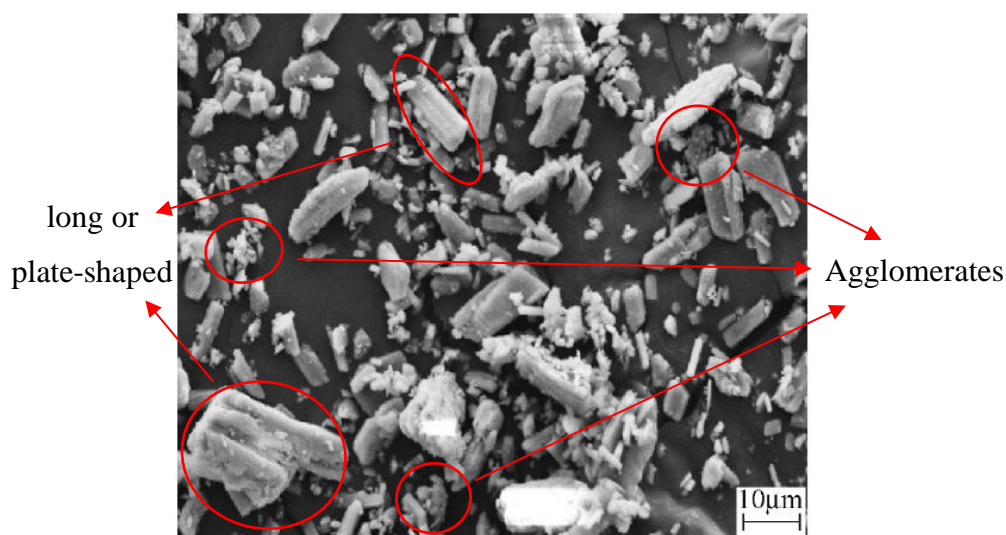
Figure 4.3: SEM Image of Products after Acid Leaching Method (Jiang, Sun and Peng, 2019).

For the hydrothermal treatment method, almost zero agglomerate could be seen from the SEM image of the products. Only strips and plate-shaped particles were observed in Figure 4.4. It indicated that almost all the iron impurities were removed by hydrothermal treatment, so the efficiency of iron in this method could achieve around 99%. In a nutshell, the hydrothermal treatment method had the best efficiency for iron extraction, followed by acid leaching and mineral carbonation methods.
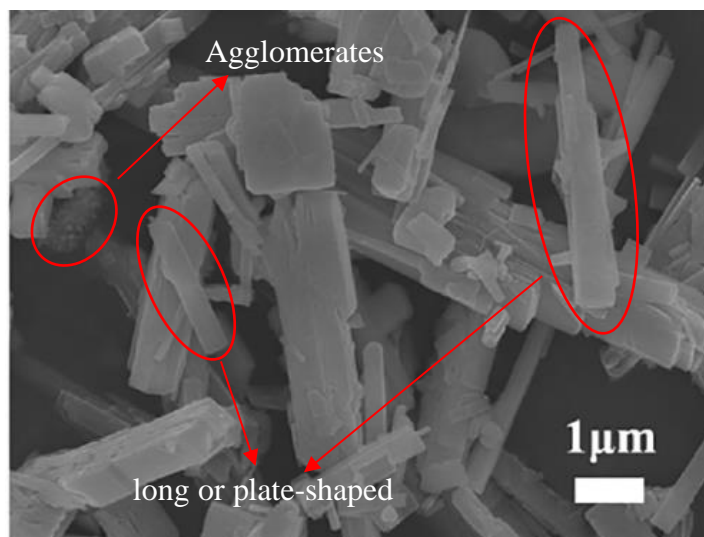
Figure 4.4: SEM Image of Products after Hydrothermal Treatment (Peng, et al., 2021).

4.2.3 Cost Aspect

The material and energy costs of each pretreatment method were performed in **Section 4.1**. From Table 4.15, the acid leaching method required the least cost of RM 5460.32, followed by hydrothermal treatment with RM 6461.85, and finally, the mineral carbonation method with the cost of RM 13040.41. However, the equipment cost, transportation cost, labour cost and product benefit were neglected in this study as these costs were subjective to different companies.

4.2.4 Summary

Table 4.16 showed the comparison of mineral carbonation, acid leaching and hydrothermal treatments with environmental, efficiency and cost aspects.

Table 4.16: Summary of All Aspects.

	Mineral Carbonation	**Acid Leaching**	**Hydrothermal Treatment**
Environmental Aspect	No impact	Moderate Impact	Moderate Impact
Efficiency Aspect	Low	Moderate	High
Cost Aspect	High	Low	Moderate

Among these three pretreatment methods, hydrothermal treatment was the most feasible method for extracting iron metal from RG for several reasons. In terms of the extraction rate of iron, it had the highest extraction rate of iron which is 99%, so the products were suitable to reutilise in other applications. Although 1.5 M HCl in the hydrothermal treatment method was more corrosive than the acid leaching method, which used only 0.5 M H_2SO_4, the negative impact on the environment was almost similar. Besides, the cost required for hydrothermal treatment was only RM 1001.53 lower than that of the acid leaching method in one tonne of red gypsum basis. However, the purity of products in hydrothermal treatment could achieve 99%, and its benefits would be higher than the products after acid leaching. Besides, the hydrothermal treatment method had the most straightforward procedures, and the equipment requirements were not complicated. Although the mineral carbonation method had no negative impact on the environment and could solve environmental issues, the extraction rate of iron and the purity of products were low, so the products were challenging to reutilise in other applications. Furthermore, the cost required in mineral carbonation was the highest among the three treatments. Thus, the hydrothermal treatment method was the best for the pretreatment method of red gypsum among these three treatment methods.

CHAPTER 5

CONCLUSIONS AND RECOMMENDATIONS

5.1 Conclusions

This report reviewed three pretreatment methods of red gypsum to extract the iron metal, including mineral carbonation, acid leaching, and hydrothermal treatment methods. The review showed that understanding and control over solid phase microstructure and iron speciation are essential for effectively extracting iron from red gypsum. The hydrothermal treatment method is the technique that can well control the solid phase microstructure and iron speciation. Therefore, the highest efficiency of extracting iron metal which was 99%, can be achieved.

Besides, the review also showed the mechanism, parameter studied, and feasibility studied for each pretreatment method. Generally, the smaller particle size of red gypsum can achieve higher efficiency as the total specific surface area of red gypsum particle becomes higher. Besides, the higher heating time or reaction time can also achieve higher efficiency as the iron impurities adsorbed on red gypsum have more time to diffuse or dissolve into the solvent. Furthermore, the solid-liquid ratio in the techniques of solid-liquid separation was crucial. The lower the solid-liquid ratio, the greater the $H_2SO_4 - H_2O$ distributed per unit mass of red gypsum, so the more conducive to the dissolution of iron impurities. Last but not least, the higher the concentration of reactants (CO_2, sulphuric acid and hydrochloric acid), the higher the efficiency can be attained.

The best pretreatment method is examined based on environmental, efficiency and cost perspectives. The material and energy cost analysis of mineral carbonation, acid leaching and hydrothermal treatment methods were RM 13040.41, RM 5460.32 and RM 6461.85, respectively. The hydrothermal treatment method was the best pretreatment method of red gypsum among these three treatment methods. It had the highest efficiency, 99%, and moderate cost required of RM 6461.85 and a moderate negative impact on environment.

5.2 Recommendations for Future Work

Under this study, all the results and data are obtained from other researchers' experiments. Therefore, it is recommended to study the parameters of hydrothermal treatment by conducting an experiment, especially the concentration of mineraliser (hydrochloric acid), to have a less negative impact on the environment. Besides, a proper separation technique to separate solid residue and acidic filtrate after hydrothermal treatment have to be studied. If the acid is adsorbed on the solid residue, it will affect the following applications, such as cement production. Furthermore, the mineral carbonation method is an environmentally friendly technique. An experiment can be conducted to study the parameters to increase efficiency so that natural gypsum can be obtained with high purity.

REFERENCES

Artha Mineral Resources, 2021. *Natural gypsum.* [online] Available at: <http://www.arthaminerals.com/natural-gypsum.htm> [Accessed 7 July 2021].

ASTM Standard, 2002. *D854:2002 Standard test methods for specific gravity of soil solids by water pycnometer.* West Conshohocken: ASTM.

ASTM Standard, 2008. *D4943:2008 Standard test method for shrinkage factors of soils by the wax method.* West Conshohocken: ASTM.

Azdarpour, A., Asadullah, M., Junin, R., Manan, M., Hamidi, H. and Mohammadian, E., 2014. Direct carbonation of red gypsum to produce solid carbonates. *Fuel Processing Technology*, 126, pp.429–434.

Azdarpour, A., Asadullah, M., Junin, R., Mohammadian, E., Hamidi, H., Daud, A.R.M. and Manan, M., 2015. Extraction of calcium from red gypsum for calcium carbonate production. *Fuel Processing Technology*, 130, pp.12–19.

Benhammada, A., Trache, D., Kesraoui, M. and Chelouche, S., 2020. Hydrothermal synthesis of hematite nanoparticles decorated on carbon mesospheres and their synergetic action on the thermal decomposition of nitrocellulose. *Nanomaterials*, 10(5), p.968.

Bernama, 2020. *Higher water tariff necessary to upgrade infrastructure.* [online] Available at: <https://www.nst.com.my/news/nation/2020/02/562532/higher-water-tariff-necessary-upgrade-infrastructure#:~:text=The current water tariff is,per 1%2C000 litres of water.> [Accessed 27 March 2022].

Blencoe, J.G., Palmer, D.A., Anovitz, L.M. and Beard, J.S., UT-Battelle, LLC, 2014. *Carbonation of metal silicates for long-term CO_2 sequestration.* U.S. Pat. 8,673,256 B2.

Boote, D.N. and Beile, P., 2005. Scholars before researchers: on the centrality of the dissertation literature review in research preparation. *Educational Researcher*, 34(6), pp.3–15.

British Standard, 1990. *BS 1377: 1990 Methods of test for soils for civil engineering purposes part 2. classification tests.* Milton Keynes: BSI.

Brocke, J.V., Simons, A., Niehaves, B., Riemer, K., Plattfaut, R. and Cleven, A., 2009. *Reconstructing the giant: On the importance of rigour in documenting the literature search process.* In: ECIS (European Conference on Information Systems). Verona, Italy, June 2006.

Chen, Q., Ding, W., Sun, H. and Peng, T., 2021. Synthesis of anhydrite from red gypsum and acidic wastewater treatment. *Journal of Cleaner Production*, 278, p.124026.

Chen, W.L., Chen, C.K., Lee, J.W., Lee, Y.L., Ju, C.P. and Lin, J.H.C., 2014. Structure, properties and animal study of a calcium phosphate/calcium sulfate composite cement. *Materials Science and Engineering C*, 37(1), pp.60–67.

Chen, Z.Y., O'Connor, W.K. and Gerdemann, S.J., 2006. Chemistry of aqueous mineral carbonation for carbon sequestration and explanation of experimental results. *Environmental Progress*, 25(2), pp.161–166.

Clark, J., 2005. *Iron and steel*. [online] Available at: <http://www.chemguide.co.uk/inorganic/extraction/iron.html> [Accessed 5 July 2021].

Cronin, C., 2011. Doing your literature review: traditional and systematic techniques. *Evaluation & Research in Education*, 24(3), pp.219–221.

Ding, M., Huang, J., Wang, L. and Zhuang, L., Shuangfeng Economic Development Zone Hefei, Anhui, P.R., 2016. *Separation and removal process of iron element in titanium gypsum*. CN Pat. 105502464 A.

Fauziah, I., Zauyah, S. and Jamal, T., 1996. Characterization and land application of red gypsum: A waste product from the titanium dioxide industry. *Science of the Total Environment*, 188(2–3), pp.243–251.

Felder, R., Rousseau, R. and Bullard, L., 2016. *Elementary Principles of Chemical Processes*. 4th ed. Hoboken, New Jersey: John Wiley & Sons.

Gázquez, M.J., Bolívar, J.P., García-Tenorio, R. and Vaca, F., 2009. Physicochemical characterization of raw materials and co-products from the titanium dioxide industry. *Journal of Hazardous Materials*, 166(2–3), pp.1429–1440.

Gazquez, M.J., Bolivar, J.P., Vaca, F., García-Tenorio, R. and Caparros, A., 2013. Evaluation of the use of TiO_2 industry red gypsum waste in cement production. *Cement and Concrete Composites*, 37(1), pp.76–81.

Gázquez, M.J., Mantero, J., Bolívar, J.P., García-Tenorio, R., Vaca, F. and Lozano, R.L., 2011. Physico-chemical and radioactive characterization of TiO_2 undissolved mud for its valorization. *Journal of Hazardous Materials*, 191(1–3), pp.269–276.

Geankoplis, C.J., Hersel, A.A. and Lepek, D.H., 2018. *Transport Processes and Separation Process Principles*. 5th ed. Hoboken, New Jersey: Prentice Hall.

Gerdemann, S.J., O'Connor, W.K., Dahlin, D.C., Penner, L.R. and Rush, H., 2007. Ex situ aqueous mineral carbonation. *Environmental Science and Technology*, 41(7), pp.2587–2593.

Global Petrol Prices, 2021. *Malaysia electricity prices*. [online] Available at: <https://www.globalpetrolprices.com/Malaysia/electricity_prices/>. [Accessed 27 March 2022].

Green, B.N., Johnson, C.D. and Adams, A., 2006. Writing narrative literature reviews for peer-reviewed journals: secrets of the trade. *Journal of Chiropractic Medicine*, 5(3), pp.101–111.

Green, D.W. and Perry, R.H., 2007. *Perry's Chemical Engineers' Handbook*. 8th ed. New York: McGraw-Hill.

Hamid, N.J.A., Kadir, A.A., Hashar, N.N.H., Pietrusiewicz, P., Nabiałek, M., Wnuk, I., Gucwa, M., Palutkiewicz, P., Hashim, A.A., Sarani, N.A., Nio, A.A., Noor, N.M. and Jez, B., 2021. Influence of gypsum waste utilization on properties and leachability of fired clay brick. *Materials*, 14(11), pp.1–11.

Herk, J.V., Pietersen, H.S. and Schuiling, R.D., 1989. Neutralization of industrial waste acids with olivine - The dissolution of forsteritic olivine at 40-70°C. *Chemical Geology*, 76(3–4), pp.341–352.

Huijgen, W.J.J., Witkamp, G.J. and Comans, R.N.J., 2006. Mechanisms of aqueous wollastonite carbonation as a possible CO_2 sequestration process. *Chemical Engineering Science*, 61(13), pp.4242–4251.

Indeed, 2021. *Learn how to calculate cost analysis*. [online] Available at: <https://www.indeed.com/career-advice/career-development/cost-analysis#:~:text=Cost analysis%2C also known as,completing that situation or project.> [Accessed 9 March 2022].

InkWorld, 2021. *Titanium dioxide market to register 8.3% CAGR from 2021-28: grand view research*. [online] Available at: <https://www.inkworldmagazine.com/contents/view_breaking-news/2021-05-31/titanium-dioxide-market-to-register-83-cagr-from-2021-28-grand-view-research/> [Accessed 7 July 2021].

Jiang, M., Sun, H. and Peng, T., 2019. Extraction of iron oxide from titanium gypsum by sulfuric acid leaching and phase transform of gypsum. *Chemical Industry and Engineering Progress*, 38(4), pp.2030–2036.

Kakizawa, M., Yamasaki, A. and Yanagisawa, Y., 2001. A new CO_2 disposal process via artificial weathering of calcium silicate accelerated by acetic acid. *Energy*, 26(4), pp.341–354.

Kamarudin, R.A. and Zakaria, M.S., 2007. The utilization of red gypsum waste for glazes. *The Malaysian Journal of Analytical Sciences*, 11(1), pp.57–64.

Karas, L., 2022. *Literature review: purpose of a literature review.* [online] Available at: <https://uscupstate.libguides.com/c.php?g=627058&p=4389968> [Accessed 28 January 2022].

Kodama, S., Nishimoto, T., Yamamoto, N., Yogo, K. and Yamada, K., 2008. Development of a new pH-swing CO_2 mineralization process with a recyclable reaction solution. *Energy*, 33(5), pp.776–784.

Koretsky, M.D., 2013. *Engineering and Chemical Thermodynamics*. 2nd ed. Hoboken, New Jersey: John Wiley & Sons.

Lee, M.G., Jang, Y.N., Ryu, K.W., Kim, W. and Bang, J.H., 2012. Mineral carbonation of flue gas desulfurization gypsum for CO_2 sequestration. *Energy*, 47(1), pp.370–377.

Lemire, R.J., Berner, U., Musikas, C., Palmer, D.A., Taylor, P., Tochiyama, O. and Perrone, J., 2013. Chemical thermodynamics of iron, Part 1 - Chemical thermodynamics volume 13a. Canada: OECD (Organisation for Economic Co-operation and Development).

Linde, 2017. *Carbon Dioxide*. [online] Available at: <https://www.linde-gas.com/en/images/LMB_Safety Advice_01_66881_tcm17-165650.pdf> [Accessed 27 March 2022].

Liu, W., Weng, C., Zheng, J., Peng, X., Zhang, J. and Lin, Z., 2019. Emerging investigator series: Treatment and recycling of heavy metals from nanosludge. *Environmental Science: Nano*, 6(6), pp.1657–1673.

Liu, W., Zheng, J., Ou, X., Liu, X., Song, Y., Tian, C., Rong, W., Shi, Z., Dang, Z. and Lin, Z., 2018. Effective extraction of CR(VI) from hazardous gypsum sludge via controlling the phase transformation and chromium species. *Environmental Science and Technology*, 52(22), pp.13336–13342.

Liu, X. and Millero, F.J., 2002. The solubility of iron in seawater. *Marine Chemistry*, 77(1), pp.43–54.

Lumen, 2022. *Strength of acids*. [online] Available at: <https://courses.lumenlearning.com/boundless-chemistry/chapter/strength-of-acids/> [Accessed 30 March 2022].

Ma, X., Yao, S., Yuan, Z., Bi, R., Wu, X., Zhang, J., Wang, S., Wang, X. and Jia, Y., 2020. Detoxification and reclamation of hydrometallurgical arsenic- and trace metals-bearing gypsum via hydrothermal recrystallization in acid solution. *Chemosphere*, 250, p.126290.

Madhusha, 2017. *Difference between hydrochloric acid and sulfuric acid*. [online] Available at: <https://pediaa.com/difference-between-hydrochloric-acid-and-sulfuric-acid/#:~:text=Main Difference – Hydrochloric Acid vs Sulfuric Acid&text=Hydrochloric acid and sulfuric acid are two strong acids.,whereas sulfuric acid is diprotic.> [Accessed 30 March 2022].

Mahazam, N. and Mohd Azmi, N.S., 2016. Evaluation of physical and chemical properties of red gypsum from Terengganu, Malaysia. *International Journal of Engineering Research & Technology*, 5(01), pp.433–436.

Mantero, J., Gazquez, M.J., Bolivar, J.P., Garcia-Tenorio, R. and Vaca, F., 2013. Radioactive characterization of the main materials involved in the titanium dioxide production process and their environmental radiological impact. *Journal of Environmental Radioactivity*, 120, pp.26–32.

Maroto-Valer, M.M., Fauth, D.J., Kuchta, M.E., Zhang, Y. and Andrésen, J.M., 2005. Activation of magnesium rich minerals as carbonation feedstock materials for CO_2 sequestration. *Fuel Processing Technology*, 86(14–15), pp.1627–1645.

Mountholyoke, 2005. *V(k). Chemical safety - Corrosive*. [online] Available at: <https://www.mtholyoke.edu/ehs/science-center-safety-handbook/vkcorrosives#:~:text=The corrosivity of acids and,with water is extremely exothermic.> [Accessed 31 March 2022].

Nest Group, 2021. *Molarity of concentrated acids & bases*. [online] Available at: <https://www.nestgrp.com/protocols/trng/molarity.shtml> [Accessed 31 March 2022].

Newton, J., 2018. *The effects of landfills on the environment*. [online] SCIENCING. Available at: <https://sciencing.com/effects-landfills-environment-8662463.html> [Accessed 7 July 2021].

NIST, 2017. *Carbon dioxide*. [online] National Institute of Standards and Technology. Available at: <https://webbook.nist.gov/cgi/cbook.cgi?Name=Decane&Units=SI> [Accessed 20 March 2022].

O'Connor, W.K., Dahlin, D.C., Rush, G.E., Dahlin, C.L. and Collins, W.K., 2001. Carbon dioxide sequestration by direct mineral carbonation: Process mineralogy of feed and products. *Minerals and Metallurgical Processing*, 19(2), pp.95–101.

Pan, Z., Wang, Y., Huang, H., Ling, Z., Dai, Y. and Ke, S., 2015. Recent development on preparation of ceramic inks in ink-jet printing. *Ceramics International*, 41(10), pp.12515–12528.

Paré, G. and Kitsiou, S., 2017. *Methods for literature reviews*. [online] Available at: <https://www.ncbi.nlm.nih.gov/books/NBK481583/> [Accessed 28 January 2022].

Park, A.H.A. and Fan, L.S., 2004. CO_2 mineral sequestration: Physically activated dissolution of serpentine and pH swing process. *Chemical Engineering Science*, 59(22–23), pp.5241–5247.

Peng, X., Zheng, J., Liu, Q., Hu, Q., Sun, X., Li, J., Liu, W. and Lin, Z., 2021. Efficient removal of iron from red gypsum via synergistic regulation of gypsum phase transformation and iron speciation. *Science of the Total Environment*, 791, p.148319.

Pérez-Moreno, S.M., Gázquez, M.J. and Bolívar, J.P., 2015. CO_2 sequestration by indirect carbonation of artificial gypsum generated in the manufacture of titanium dioxide pigments. *Chemical Engineering Journal*, 262, pp.737–746.

Pharmacompass, 2022a. *Carbon dioxide*. [online] Available at: <https://www.pharmacompass.com/active-pharmaceutical-ingredients/carbon-dioxide> [Accessed 27 March 2022].

Pharmacompass, 2022b. *Hydrochloric acid*. [online] Available at: <https://www.pharmacompass.com/active-pharmaceutical-ingredients/hydrochloric-acid> [Accessed 27 March 2022].

Pharmacompass, 2022c. *Sulphuric acid*. [online] Available at: <https://www.pharmacompass.com/active-pharmaceutical-ingredients/sulphuric-acid> [Accessed 27 March 2022].

Pillai, V.N., 2020. *Research Methodology: Literature Review*. [online] Available at: <https://www.researchgate.net/publication/339716552_Research_Methodology_Literature_Review> [Accessed 28 January 2022].

Rahmani, O., Tyrer, M. and Junin, R., 2014. Calcite precipitation from by-product red gypsum in aqueous carbonation process. *RSC Advances*, 4(85), pp.45548–45557.

Riahi, K., Rubin, E.S. and Schrattenholzer, L., 2004. Prospects for carbon capture and sequestration technologies assuming their technological learning. *Energy*, 29(9–10), pp.1309–1318.

Sahoo, S., Agarwal, K., Singh, A., Polke, B. and Raha, K., 2011. Characterization of γ- and α-Fe_2O_3 nano powders synthesized by emulsion precipitation-calcination route and rheological behaviour of α-Fe_2O_3. *International Journal of Engineering, Science and Technology*, 2(8), pp.118-126.

Scottish Environment Protection Agency (SEPA), 2009. The disposal in landfills for non-hazardous waste of gypsum wastes. [online] Available at: <https://www.sepa.org.uk/media/28998/technical-guidance-note-disposal-of-gypsum-in-landfills.pdf> [Accessed 27 March 2022].

Seider, W.D., Lewin, D.R., Seader, J.D., Widagdo, S., Gani, R. and Ng, K.M., 2017. *Product and process design principles - synthesis, analysis and evaluation,* 4th ed. New York: John Wiley & Sons, Inc.

Snyder, H., 2019. Literature review as a research methodology: An overview and guidelines. *Journal of Business Research*, 104, pp.333–339.

Stefánsson, A., 2007. Iron (III) hydrolysis and solubility at 25 °C. *Environmental Science & Technology*, 41(17), pp.6117–61123.

Teir, S., Revitzer, H., Eloneva, S., Fogelholm, C.J. and Zevenhoven, R., 2007. Dissolution of natural serpentinite in mineral and organic acids. *International Journal of Mineral Processing*, 83(1–2), pp.36–46.

Templier, M. and Paré, G., 2015. A framework for guiding and evaluating literature reviews. *Communications of the Association for Information Systems*, 37(6), pp.112–137.

Tooze, J.F., Noble, B.C. and August, A.E., 2003. *Red gypsum in civil engineering applications*. WO Pat. 03/070657 A1.

TOPPR, 2022. *Why is ammonium hydroxide used in qualitative analysis?* [online] Available at: <https://www.toppr.com/ask/en-my/question/why-is-ammonium-hydroxide-used-in-qualitative-analysis-give-two-equations-to-justify-your-answer/> [Accessed 3 February 2022].

Wu, H., Feng, Y., Li, H., He, S. and Bian, Z., 2019. Red gypsum utilization and acidic wastewater treatment based on metal self-enrichment process. *Science of the Total Environment*, 691, pp.9–15.

Zhang, J., Yan, Y., Hu, Z., Xie, X. and Yang, L., 2019. Properties and hydration behavior of Ti-extracted residues-red gypsum based cementitious materials. *Construction and Building Materials*, 218, pp.610–617.

Zhang, Y., Wang, F., Huang, H., Guo, Y., Li, B., Liu, Y. and Chu, P.K., 2016. Gypsum blocks produced from TiO_2 production by-products. *Environmental Technology*, 37(9), pp.1097–1100.

Zheng, J., Li, J., Ling, L., Liu, X., Kong, S., Liao, H., Liu, W., Ning, P. and Lin, Z., 2019. Crystal regulation of gypsum via hydrothermal treatment with hydrogen ion for Cr(VI) extraction. *Journal of Hazardous Materials*, 390, p.120614.

Zumdahl, 2003. *Table of Acids with Ka and pKa Values*. [online] Available at: <http://clas.sa.ucsb.edu/staff/Resource Folder/Chem109ABC/Acid, Base Strength/Table of Acids w Kas and pKas.pdf> [Accessed 27 March 2022].

APPENDICES

Appendix A: Heat Capacity Data

The heat capacity data of all materials involved in the three studied treatment methods are tabulated in Table A-1, Table A-2 and Table A-3. The heat capacity data of $Fe(OH)_2$, $Fe(OH)_3$, $Fe_2(SO_4)_3$ and $FeCO_3$ are tabulated in Table A-1 and retrieved from Lemire et al. (2013) while the heat capacity data of CO_2, H_2O and H_2SO_4 are tabulated in Table A-2 and retrieved from Koretsky (2013). Besides, the heat capacity data of $CaCO_3$ and $CaSO_4$ is retrieved from Felder, Rousseau and Bullard (2016), and Green and Perry (2007) respectively as shown in Table A-3.

Table A-1: Heat Capacity Data of $Fe(OH)_2$, $Fe(OH)_3$, $Fe_2(SO_4)_3$ and $FeCO_3$ (Lemire, et al., 2013).

Formula: $C_p[\text{J/K} \cdot \text{mol}] = A + BT + CT^2 + DT^{-1} + ET^{-2}$ with T in [K]							
Chemicals	A	B	C	D	E	T_{min}(K)	T_{max}(K)
$Fe(OH)_2$				90 J/K $\cdot$ mol			
$Fe(OH)_3$				152 J/K $\cdot$ mol			
$Fe_2(SO_4)_3$	202.96	0.3315	0	0	-2.567×10^6	230	500
$FeCO_3$	52.39	0.1258	-3.308×10^{-5}	0	-4.004×10^5	250	395

Table A-2: Heat Capacity Data of CO_2, H_2O and H_2SO_4 (Koretsky, 2013).

Formula: $\frac{C_p}{R}$ [J/K · mol] $= A + BT + CT^2 + DT^{-2} + ET^3$ with T in [K]

Chemicals	A	B	C	D	E	T_{min} (K)	T_{max} (K)
CO_2	5.457	1.045×10^{-3}	0	-1.157×10^{-5}	0	298	2000
H_2O	3.47	1.45×10^{-3}	0	1.21×10^{-6}	0	298	2000
H_2SO_4	16.731	1.875×10^{-3}	0	0	0	-	-

Table A-3: Heat Capacity Data of $CaCO_3$ and $CaSO_4$ (Felder, Rousseau and Bullard, 2016; Green and Perry, 2007).

Formula: C_p [kJ/K · mol] $= A + BT + CT^{-2}$ with T in [K]

Chemicals	A	B	C	T_{min} (K)	T_{max} (K)
$CaCO_3$	8.234×10^{-2}	4.975×10^{-5}	1.287×10^3	273	1033

Formula: C_p [cal/K · mol] $= A + BT + CT^{-2}$ with T in [K]

Chemicals	A	B	C	T_{min} (K)	T_{max} (K)
$CaSO_4$	18.52	2.197×10^{-2}	-1.568×10^5	273	1373

Four sample calculations with different equations are performed in this section. Firstly, the calculation of heat capacity of $Fe_2(SO_4)_3$ from Table A-1 is performed.

$$C_p = \int_{T_{in}}^{T_{out}} A + BT + CT^2 + DT^{-1} + ET^{-2}\ dT$$

$$C_p = \left[A(T_{out} - T_{in}) + \frac{B(T_{out}^2 - T_{in}^2)}{2} + \frac{C(T_{out}^3 - T_{in}^3)}{3} + D\left(\ln\frac{T_{out}}{T_{in}}\right) \right.$$
$$\left. - E\left(\frac{1}{T_{out}} - \frac{1}{T_{in}}\right) \right]$$

Taking $T_{in} = 70\ °C$ and $T_{out} = 30\ °C$ in the **Section 4.1.2.2** of cooling down the product to the ambient temperature of $30\ °C$.

$$C_p = \left[202.96 \times (303.15 - 343.15) + \frac{0.3315 \times (303.15^2 - 343.15^2)}{2} \right.$$
$$\left. - (-2.567 \times 10^6)\left(\frac{1}{303.15} - \frac{1}{343.15}\right) \right]$$
$$C_p = -11417\ J/mol \cdot K$$

Secondly, the calculation of heat capacity of CO_2 from Table A-2 is performed.

$$C_p = R \int_{T_{in}}^{T_{out}} A + BT + CT^2 + DT^{-2} + ET^3\ dT$$

$$C_p = R\left[A(T_{out} - T_{in}) + \frac{B(T_{out}^2 - T_{in}^2)}{2} + \frac{C(T_{out}^3 - T_{in}^3)}{3} - D\left(\frac{1}{T_{out}} - \frac{1}{T_{in}}\right) \right.$$
$$\left. + \frac{E(T_{out}^4 - T_{in}^4)}{4} \right]$$

Taking $T_{in} = 200\ °C$ and $T_{out} = 30\ °C$ in the **Section 4.1.1.2** of cooling down the product to the ambient temperature of $30\ °C$.

$$C_p = 8.314 \left[5.457 \times (303.15 - 473.15) \right.$$

$$+ \frac{(1.045 \times 10^{-3})(303.15^2 - 473.15^2)}{2}$$

$$\left. - (-1.157 \times 10^{-5}) \left(\frac{1}{303.15} - \frac{1}{473.15} \right) \right]$$

$$C_p = -8286 \text{ J/mol} \cdot \text{K}$$

Thirdly, the calculation of heat capacity of $CaCO_3$ from Table A-3 is performed.

$$C_p = \int_{T_{in}}^{T_{out}} A + BT + CT^{-2} \, dT$$

$$C_p = \left[A(T_{out} - T_{in}) + \frac{B(T_{out}^2 - T_{in}^2)}{2} - C \left(\frac{1}{T_{out}} - \frac{1}{T_{in}} \right) \right]$$

Taking $T_{in} = 200$ °C and $T_{out} = 30$ °C in the **Section 4.1.1.2** of cooling down the product to the ambient temperature of 30 °C.

$$C_p = \left[(8.234 \times 10^{-2}) \times (303.15 - 473.15) \right.$$

$$+ \frac{(4.975 \times 10^{-5})(303.15^2 - 473.15^2)}{2}$$

$$\left. - (-1.287 \times 10^3) \left(\frac{1}{303.15} - \frac{1}{473.15} \right) \right]$$

$$C_p = -15.755 \text{ kJ/mol} \cdot \text{K} \times \frac{1000 \text{ J}}{\text{kJ}}$$

$$C_p = -15755 \text{ J/mol} \cdot \text{K}$$

Lastly, the calculation of heat capacity of $CaSO_4$ from Table A-3 is performed.

$$C_p = \int_{T_{in}}^{T_{out}} A + BT + CT^{-2} \, dT$$

$$C_p = \left[A(T_{out} - T_{in}) + \frac{B(T_{out}^2 - T_{in}^2)}{2} - C\left(\frac{1}{T_{out}} - \frac{1}{T_{in}}\right) \right]$$

Taking $T_{in} = 200$ °C and $T_{out} = 30$ °C in the **Section 4.1.1.2** of cooling down the product to the ambient temperature of 30 °C.

$$C_p = \left[18.52 \times (303.15 - 473.15) + \frac{(2.197 \times 10^{-2})(303.15^2 - 473.15^2)}{2} \right.$$

$$\left. - (-1.568 \times 10^5)\left(\frac{1}{303.15} - \frac{1}{473.15}\right) \right]$$

$$C_p = -4412.26 \text{ cal/mol} \cdot K \times \frac{4.184 \text{ J}}{\text{cal}}$$

$$C_p = -18461 \text{ J/mol} \cdot K$$